Modelling forces in milling screw rotors

by

Xi Wang
B.Eng, University of Victoria, 2022

A Thesis Submitted in Partial Fulfillment of the
Requirements for the Degree of

MASTER OF APPLIED SCIENCE

in the Department of Mechanical Engineering

Modelling forces in milling screw rotors

by

Xi Wang
B.Eng, University of Victoria, 2022

Supervisory Committee

Dr. Keivan Ahmadi, Supervisor
(Department of Mechanical Engineering)

Dr. Zuomin Dong, Departmental Member
(Department of Mechanical Engineering)

ABSTRACT

The deflections of screw rotors under machining forces cause mismatch between the male and female rotors and, consequently, accelerated wear and suboptimal efficiency in their performance. Optimizing the machining process to minimize the generated forces and accounting for the resulting mismatch in the design of the rotor profile requires accurately computing the machining forces in computer simulations. Virtual machining systems combine graphics-based computation of the Cutter-Workpiece Engagement (CWE) with the physics-based models of machining mechanics to simulate the forces during complex machining processes. However, because of the high computational load of graphical simulations, virtual machining is not suitable for the repetitive force simulations that are required for optimizing the design and manufacturing of rotors. In this work, we present a new method that simulates screw milling forces based on the process kinematics instead of graphical simulations.

Utilizing mathematical equations that describe the process kinematics, the theoretical rotor profile is determined for feasible combinations of cutting tool profile, setup angle, and centre distance. Subsequently, to find the milling forces, the cutting edge is discretized into multiple small edge segments and a mechanistic cutting force model is used to determine the local cutting forces at each segment. After geometric and kinematic transformations of these local forces, the screw milling forces are obtained for each roughing and finishing pass. Instead of graphics-based methods, the engagement conditions between the cutter and workpiece are determined by the ensemble of 2D rotor and tool profiles; as a result, the computational efficiency is increased substantially.

The semi-analytical nature of the presented method allows for computing the forces with arbitrary resolution within a reasonable time. The accuracy and efficiency of the presented method is verified by comparing the simulated forces against a dexel-based virtual machining system.

Contents

Supervisory Committee **ii**

Abstract **iii**

Contents **iv**

List of Tables **vi**

List of Figures **vii**

Acronyms **ix**

Acknowledgements **x**

1 Thesis Overview **1**

1.1 Introduction 1

1.2 Research Object 3

1.3 Summary of Contributions 4

1.4 Thesis Organization 4

2 Literature Review **5**

2.1 Modelling Machining Forces 5

2.2 Cutter Workpiece Engagement 8

3 Geometry and Kinematics **13**

3.1 Example 17

4 Milling Forces **22**

4.1 Cutter-Workpiece Engagement (CWE) 24

4.2 Example 26

5 Conclusion and Future Work **33**

A Specifications in Dexel-based Method **39**

A.1 Profile Prediction 39

A.2 Forces Simulation 41

A.3 Sensitivity Analysis 42

B Bibliography **44**

List of Tables

Table 3.1 Geometrical and Machining Parameters 18

Table 5.1 Maximum Cutting Forces in each pass 34
Table 5.2 Cutter maximum deflection in the tool coordinate system 38

List of Figures

Figure 1.1 Twin screw air compressor. (a) compressor working inside the chamber, (b) meshed male and female screw rotors [1] 2
Figure 1.2 Dexel-based method used for modelling milling process [2] . . . 3

Figure 2.1 Universal slip line model and six previous models [3] 6
Figure 2.2 Three basic chip types. (a) discontinuous chip, (b) continuous chip without built-up edge, (c) continuous chip with built-up edge [4] 7
Figure 2.3 Drill edge geometry. (a) top view of the drill, (b) side view of the drill [5] 8
Figure 2.4 Geometrical modelling techniques. A. Voxel-based method, B. Z-buffer method, C. B-Rep method, D. CSG method [6] 9
Figure 2.5 Modelling techniques for gear manufacturing, A. gear shaping by dexel-based method, B. gear hobbing by dexel-based method, C. gear skiving by solid modelling method [7, 8, 9] 10
Figure 2.6 Mathematical model for helix groove machining [10] 11

Figure 3.1 Screw milling setup. (a) tool and rotor frames, (b) relative motions of the tool and rotor, (c) tool profile, (d) rotor profile . . . 14
Figure 3.2 Illustration of Guo and Tang's kinematic model [11] 15
Figure 3.3 Insert profile defined by discrete points for the kinematic model and dexel-based model 17
Figure 3.4 Comparison of the machined profile obtained from the kinematic model and dexel-based simulations 19
Figure 3.5 Potential misalignment between the tool and workpiece 20
Figure 3.6 Sensitivity analysis for different types of misalignment 21

Figure 4.1 Local forces acting on the cutting edges 23

Figure 4.2 Surface boundaries. (a) machined surface and swept surface, (b) engaged segments under surface boundaries 24
Figure 4.3 Overall forces in Z_t axis 28
Figure 4.4 Overall forces in Y_t Axis 29
Figure 4.5 Overall forces in X_t Axis 30
Figure 4.6 Maximum chip thickness 31
Figure 4.7 Comparison of the simulation time from the kinematic model and dexel-based model 32

Figure 5.1 Tool FEM Assembly 34
Figure 5.2 Maximum tool deflections in Z_t axis 35
Figure 5.3 Maximum tool deflections in Y_t axis 36
Figure 5.4 Maximum tool deflections in X_t axis 37

Figure A.1 Screw milling process in the dexel-based method 40
Figure A.2 Post processes in CAD software. (a). exporting the rotor model in STL format, (b). converting the rotor model in meshed solid body, (c). finding the cross-section perpendicular to the rotor axis, (d). transferring the data points of groove feature to spreadsheet 41
Figure A.3 Cutting forces and cutter contact area in MACHpro 42
Figure A.4 Rotor model used in sensitivity analysis 43

ACRONYMS

B-Rep Boundary Representation

CAD Computer Aided Design

CAM Computer Aided Manufacturing

CL Cutter Location

CNC Computer Numerical Control

CSG Constructive Solid Geometry

CWE Cutter-Workpiece Engagement

FEM Finite Element Modelling

NSERC Natural Sciences and Engineering Research Council of Canada

STL Standard Tessellation Language

TCP Tool Center Point

VMS Virtual Machining Systems

ACKNOWLEDGEMENTS

This research was funded by VMAC Global Technology Inc. and the Natural Sciences and Engineering Research Council of Canada (NSERC). The authors would like to thank Mrs. Drew Manson and Barry Fitzgerald for their support.

Chapter 1

Thesis Overview

1.1 Introduction

Rotary screw air compressors are widely used in diverse industrial applications, such as providing pneumatic power or processing gas extraction [1]. They show advantages in providing continuous air demand, generating powerful pneumatic power and working in mobile conditions. Compared to traditional air compressors, the rotary screw air compressor is efficient, reliable and compact. Fig. 1.1 shows the twin screw air compressor which comprises male and female rotors. The mated rotors are the most critical components inside those types of compressors. When the compressor is working, the outside air is trapped in the chamber and moves through the helical lobe by the rotation of the meshed screw rotors. The volume of air is reduced when it travels along the length of rotors and the pressured air exists at the outlet port of the compressor. The efficiency of the air volume reduction is highly connected with the rotor profiles and the rotor geometry parameters such as length, diameter, wrap angle, and clearance between the two meshed rotors [12]. Computer Numerical Control (CNC) machine tools are usually used to make complex rotor profiles. However, the clearance between the two meshed rotors needs to be considered carefully when designing screw rotor profiles.

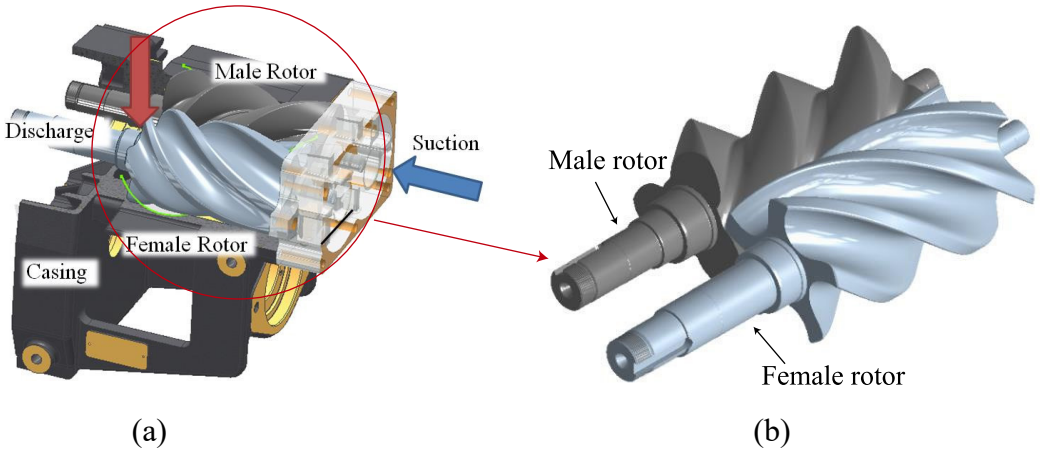

Figure 1.1: Twin screw air compressor. (a) compressor working inside the chamber, (b) meshed male and female screw rotors [1]

The design of the screw rotor profile starts by assuming zero-clearance between the two engaged rotors. If the zero-clearance design is manufactured, thermal deformations and manufacturing errors will cause interferences between the paired rotors in operation. To prevent interferences, sufficient clearance is considered between the male and female components. Excessive clearance, however, causes backlash and leakage, which undermines the volumetric efficiency of the compressor. Therefore, it is a challenge to determine the optimized clearance to achieve the balance for maximizing the air volume reduction efficiency of the compressor as well as leaving sufficient space for two engaged rotors during their operation. If a value between zero-clearance and sufficient clearance could be found, the compressor performance will increase and the cost will reduce by a longer operation life.

To design the optimized rotor profile clearance, the knowledge of the rotor profile deviations due to manufacturing errors is critical. The current practice to determine the contribution of manufacturing errors to rotor profile deviations, and compensating for them in the design stage, involves numerous costly trials and errors which may not lead to optimum design of the rotor and its manufacturing process. Besides, the physics of the process, such as generated forces, vibrations and the resulting tool and workpiece deformation is another significant part need to be analyzed. If considering zero cutting forces, the deviated profile is simple to be obtained by the manufacturing misalignment. However, the tool deflections caused by the cutting forces also result in significant profile deviations. Thus, it is important to compute the milling forces

and account for the resulting deflections when designing the rotor.

The computer simulations of machining processes, known as Virtual Machining Systems (VMS), are widely used to verify the shape of the finished part or to detect collisions and kinematically infeasible tool motions. MACHpro, as an example, is a commercial virtual machining software that can be used to predict the rotor profiles and the resulting milling forces. However, most of the VMS use computationally intensive graphics-based methods (e.g. dexels, solid modelling) to determine the geometry of engagement between the tool and the workpiece, known as Cutter-Workpiece Engagement (CWE). The high computation cost becomes inhibiting when the simulations have to be repeated many times in design optimization.

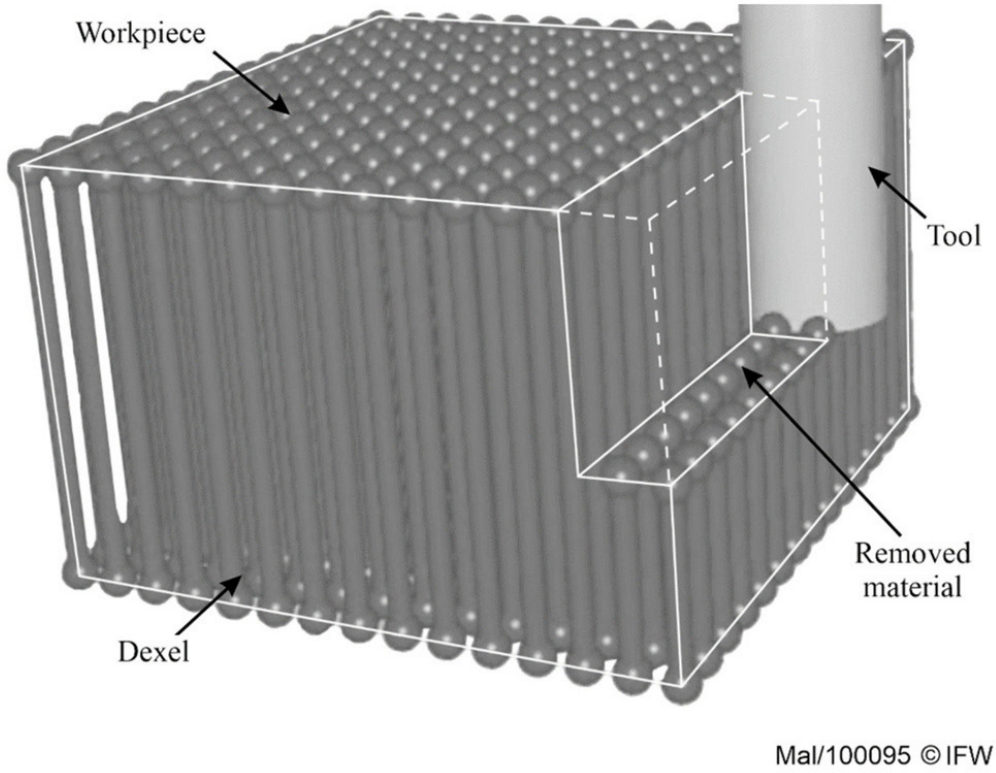

Figure 1.2: Dexel-based method used for modelling milling process [2]

1.2 Research Object

The objective of this research is to develop a computationally efficient method that computes the profile of the machined rotor as well as the forces that are generated

during its milling. To achieve this objective, computationally intensive graphics-based CWE computation is replaced by a semi-analytical kinematics-based method. The accuracy and computational efficiency of the new method will be validated by comparison to a commercial virtual machining software, MACHpro.

1.3 Summary of Contributions

The main contribution of this work is the new computationally efficient kinematics-based method for computing the milling forces in the screw rotor milling process. The rotor profile and cutting forces are predicted in the computer environment before starting the physical machining processes. The rotor profiles calculated in the kinematic model provide a quick preview of the final shape of the machined rotors. The sensitivity analysis of the profile deviation and manufacturing misalignment provide a guideline to show which type of geometry error has critical effects on the rotor profiles. The cutter maximum deflections for each pass are found by implementing the maximum cutting forces into the Finite Element Modelling (FEM) method. The deflection results are accessible for future dynamic analysis.

1.4 Thesis Organization

In Chapter 2, the literature review is presented to show the available technologies for modelling the machining forces and finding the CWE. In Chapter 3, the kinematic model is generated and the geometry and kinematic of this model are discussed. The sensitivity of the rotor profile deviation to setup misalignment is studied and the results are compared to those obtained by a multi-dexel graphics method in commercial VMS software. In Chapter 4, the cutting forces for each pass are calculated and compared with the results of the forces in the multi-dexel VMS software. In Chapter 5, the summary and future work of the research are presented.

Chapter 2

Literature Review

Rotary screw air compressors are more efficient than the traditional compressors in refrigeration and air-conditioning systems. Paired male and female screw rotors, which are considered the most critical components of the compressor, are usually manufactured by milling. While designing sufficient clearance between the paired rotors is essential for avoiding backlash or thermal interferences, the final clearance usually deviates from its nominal design due to the tool or rotor's deflection under milling forces. To minimize those deflections, the machining parameters must be optimized by simulating the forces under various machining conditions. Force simulations can also be used to determine the resulting deflections and account for them during the design of the rotor profile.

2.1 Modelling Machining Forces

A comprehensive review of modelling machining forces was presented by Arrazola et al [13]. This review introduced two main cutting force modelling techniques, analytical and numerical modellings. Slip-line field is established based on the analytical modelling method. It is developed from Merchant's early shear plane model [14] to a universal slip-line model by Fang et al. [3]. Furthermore, an orthogonal micro-cutting process is generated by Jin and Altintas [15]. Fig. 2.1 shows the development of the split line model. The Finite Element Modelling (FEM) method is one of the approaches for numerical modelling techniques and is categorized into the Lagrangian mesh or Eulerian mesh based on the type of mathematical formulation [13].

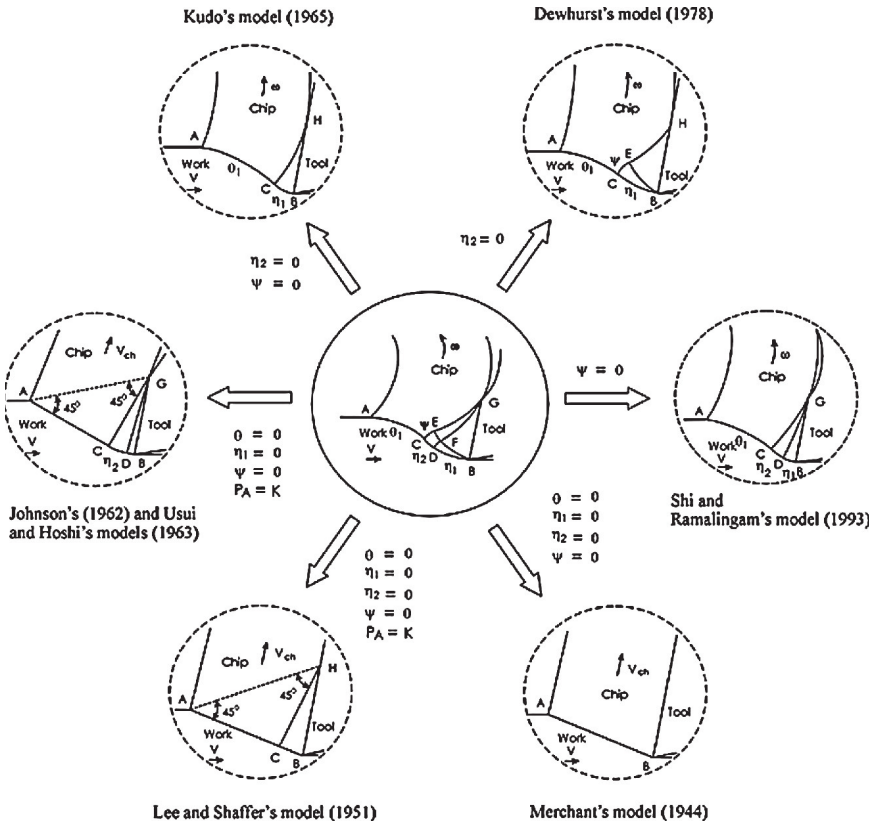

Figure 2.1: Universal slip line model and six previous models [3]

The fundamental works of Merchant [4] or Lee and Schafer [16] are among the most notable models that describe the relationship between the forces and uncut chip geometry. Merchant's model relates the cutting force system with the chip geometry under the orthogonal cutting situation [4]. The chip is considered continuous and without a built-up edge, shown as Fig. 2.2. Lee and Schafer developed a model to analytically express the cutting forces, chip thickness and chip deformation concerning the tool geometry under orthogonal machining [16]. Those fundamental models can be used directly to simulate the forces in simple single-point cutting operations such as shaping, but they also can be used as building blocks to simulate the forces in other, more complex, machining operations.

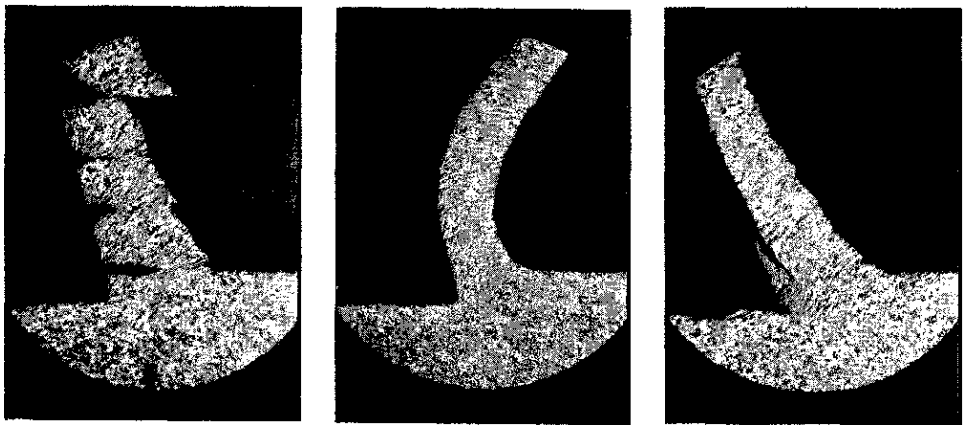

Figure 2.2: Three basic chip types. (a) discontinuous chip, (b) continuous chip without built-up edge, (c) continuous chip with built-up edge [4]

The common approach for modelling forces in general machining operations (e.g. milling or drilling) is to discretize the cutting edge geometry and its movement trajectory into smaller spacial and temporal elements and treat each element as a fundamental cutting unit that performs a basic chip generation action. The overall forces are then computed by summing the forces applied to each element after appropriate geometrical and kinematic transformations. Following this approach, Kaymakci et al. [17] presented a unified machining force model that is adaptable to the kinematics and geometry of general machining operations such as turning, milling, and drilling. A similar approach has also been adopted to simulate forces in milling and drilling with arbitrary tool geometries. Engin and Altintas [18] developed a mathematical model of the most widely used helical end mills to predict cutting forces and vibrations. The profile of the cutter edge can be determined by predefined geometric parameters. They also extended this model to the inserted cutters [19]. The inserts are mathematically defined in various shapes, such as rectangular or convex triangular. Ahmadi and Savilov [5] presented an approach to modelling the cutting edge geometry of arbitrary edge drills by parametric curve equations. Fig. 2.3 shows the drill edge geometry expressed by the 3D polynomial equation and the cutting forces in tangential, radial and axial directions.

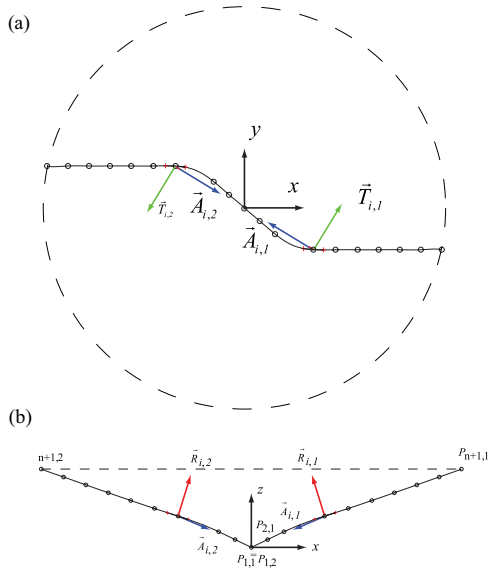

Figure 2.3: Drill edge geometry. (a) top view of the drill, (b) side view of the drill [5]

2.2 Cutter Workpiece Engagement

In operations such as 5-axis milling where Cutter-Workpiece Engagement (CWE) geometry is complex and time-varying, this generalized force modelling approach must be combined with graphics-based process simulations to determine instantaneous uncut chip geometry and the parts of the cutting edge that is engaged with the material [6]. One solution is the solid modelling method such as the Constructive Solid Geometry (CSG) and Boundary representation (B-Rep) methods conducted in Computer-Aided Design (CAD) and Computer Aided Manufacturing (CAM) environment [6]. Yip-Hoi and Huang presented an accurate process modelling to calculate the CWE geometry generated by end milling by the CSG method [20]. This modelling kernel has the highest accuracy in predicting the chip geometry and forces, however, it is computationally intensive. Other geometrical modelling techniques such as Voxel-, Dexel-, and Z-buffer-based methods [6, 21, 22], which are also called discrete volume representation, can be used to compute the CWE as well. Weinert developed a discrete volume model to simulate the milling process in sculptured surfaces [21]. This method improved the computation efficiency by excluding unnecessary memory loads.

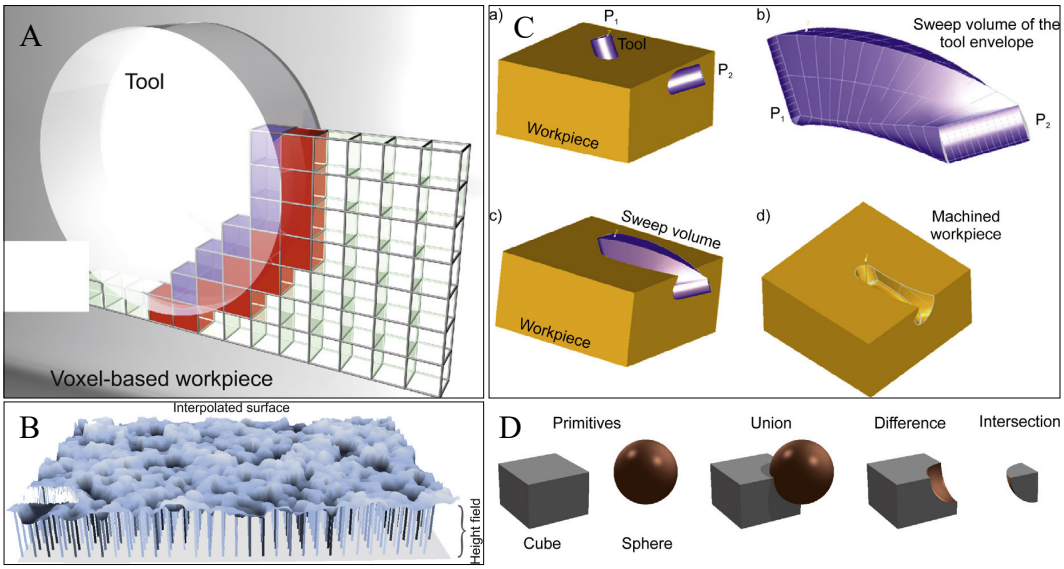

Figure 2.4: Geometrical modelling techniques. A. Voxel-based method, B. Z-buffer method, C. B-Rep method, D. CSG method [6]

To the best of our knowledge, these force simulation methods have not been used for screw-rotor milling but, it has been used to simulate the forces in operations that closely resemble the kinematics of screw-rotor milling. For example, the forces in gear hobbing, shaping, and power skiving operations have been simulated by using the multi-dexel method to determine the CWE geometry. Erkorkmaz et al. [7] predicted the CWE geometry and cutting forces at each time step by the dexel-based method in the gear shaping process. This approach shows the advantages in both the computation efficiency as well as the prediction accuracy. Katz et al. [23] extended this gear shaping study to generate complete 3-dimensional chip geometry and predict forces at any time in the shaping process. McCloskey et al. [24] and Azvar et al. [25] implemented a similar dexel-based model in the power skiving process and gear hobbing operation respectively. Klocke et al. [8] comprised the penetration calculation to the discretized representation in the gear hobbing process. The chip geometry in the gear operations can be also captured by the solid modelling method. Antoniadis [26] presented the method to determine the non-deformed chip and the developing cutting forces via CAD software in gear skiving. Tapoglou [9] demonstrated an approach in gear skiving under a CAD environment which able to provide a more accurate prediction. Fig. 2.5 shows the dexel-based and solid modelling methods in gear shaping, power skiving and hobbing.

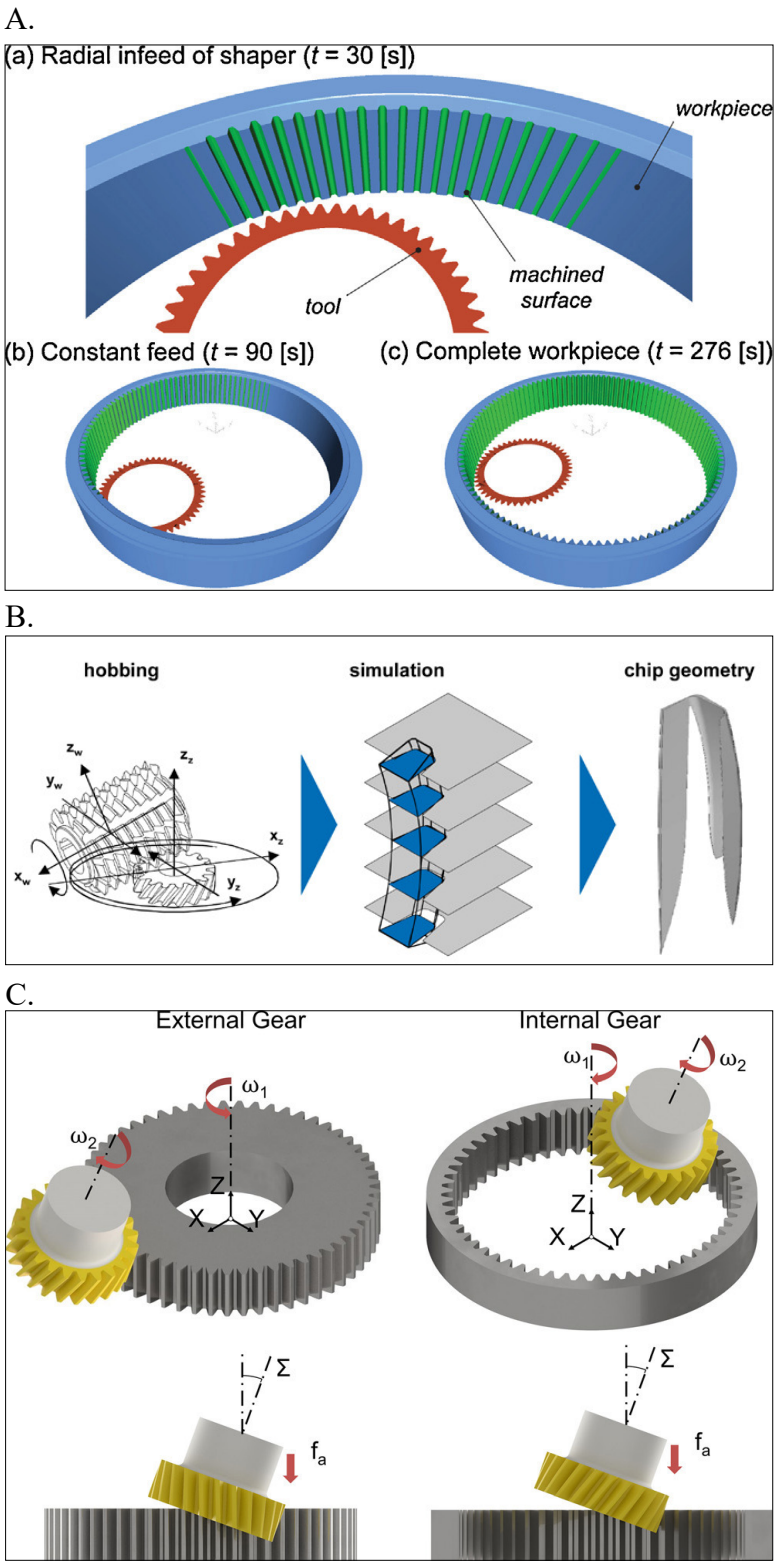

Figure 2.5: Modelling techniques for gear manufacturing, A. gear shaping by dexel-based method, B. gear hobbing by dexel-based method, C. gear skiving by solid modelling method [7, 8, 9]

However, the graphics-based methods impose large and sometimes prohibiting computational and memory load to the force simulation process [7]. The high computational load becomes even a more critical problem when force simulations are repeated over and over to optimize the design parameters of the rotor and its machining conditions. Hence, analytical methods are more beneficial in predicting chip geometry and forces in the screw rotor milling compared to the numerical methods. Hsieh [10] developed a mathematical model to analyze helical groove machining by a disk-type cutter. Seth and Malkin's model of helical groove milling kinematics relates the profile of the machined groove to the profile of the disk-shaped milling tool and the relative orientations of the tool and workpiece in the 3D space [27]. Guo and Tang [11] applied this kinematic model to determine the manufacturability of the designed screw-rotor profile and the sensitivity of the machined profile to the tool or workpiece misalignment [11, 28]. As a result, Guo and Tang's model can be used as a virtual machining system to simulate the geometry of the machined rotor, however, without considering the machining forces and their influence on the machined geometry.

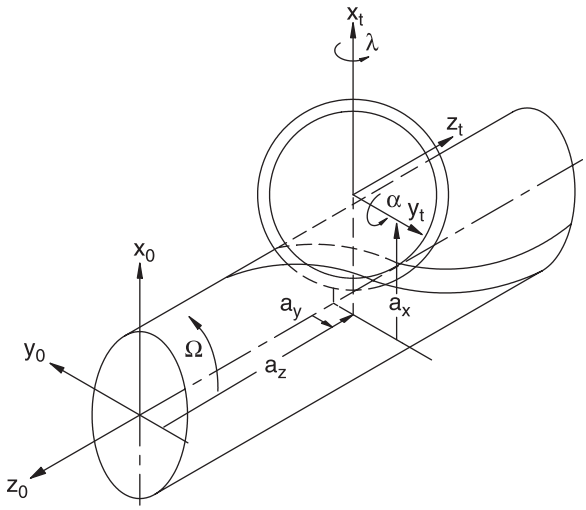

Figure 2.6: Mathematical model for helix groove machining [10]

In this thesis, Guo and Tang's kinematics model is used to determine the CWE, and then it is combined with a mechanistic force model to simulate the forces. As a result, in addition to the rotor profile, the machining forces can also be simulated semi-analytically as well. Because the CWE geometry is computed using the kinematics model of the process and not graphically, the presented method can simulate the forces with arbitrary resolution within a reasonable time. The semi-analytical nature of the presented method allows for its efficient implementation in the rotor design

or machining optimization algorithms. In chapter 3, the geometry and kinematics of the screw-rotor milling process is introduced. A case study is also presented to show the comparison of the rotor profiles computed by the kinematics model and a multi-dexel graphics method. The kinematics model is then used in chapter 4 to present a semi-analytical force simulation method. This section also validates the efficiency and accuracy of the presented force simulation method by comparing it against the forces simulated by a virtual machining software that uses a multi-dexel graphics method to obtain CWE.

Chapter 3

Geometry and Kinematics

Consider the screw rotor milling setup shown in Figs. 3.1 (a) and (b). The cutter with radius R_t is mounted in the spindle and rotates at ω_c radians per second. The rotor with radius R_r and length L_r is mounted on the table and rotates at ω_r radians per second. The angle between the axes of the rotor and cutter, denoted α, is known as the setup angle. The vertical distance between these two axes is referred to as center distance c. The coordinate frame $X_rY_rZ_r$ is fixed at the rotor center point O_r and the tool coordinate frame $X_tY_tZ_t$ is fixed at the Tool Center Point (TCP) O_t.

Helical grooves are generated by the linear motion of the TCP parallel to the rotor's axis combined with the rotational motion of the rotor around its axis. The linear speed of the TCP (V_l) is synchronized with the rotary speed of the rotor (ω_r) to generate grooves at θ helix angle, as follows:

$$\omega_r = \frac{V_l}{R_r \tan\theta} \tag{3.1}$$

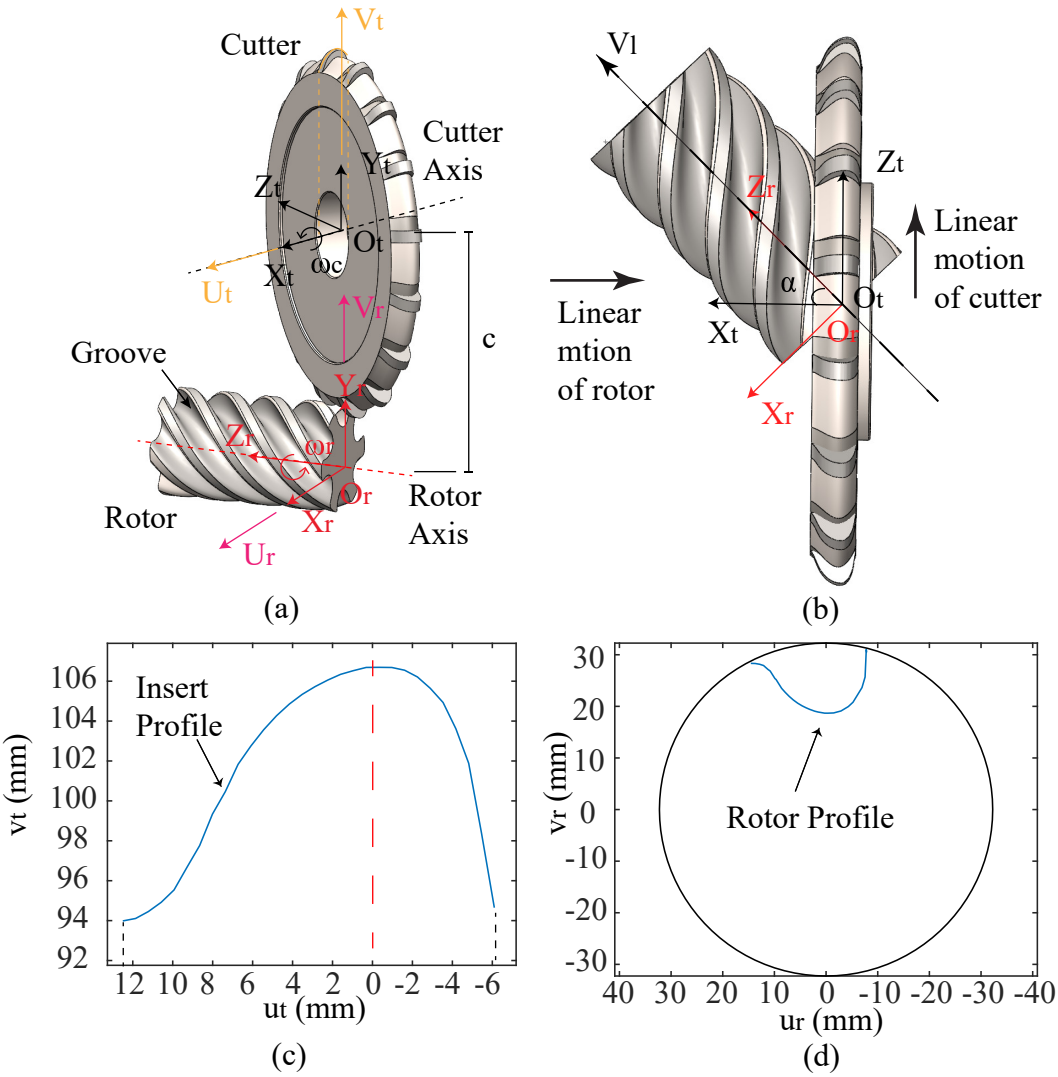

Figure 3.1: Screw milling setup. (a) tool and rotor frames, (b) relative motions of the tool and rotor, (c) tool profile, (d) rotor profile

The effective feedrate is determined by the superposition of linear and rotary velocities of the TCP and rotor, respectively:

$$f = \sqrt{V_l^2 + (c - R_t)^2 \omega_r^2} \tag{3.2}$$

The same trajectory is repeated multiple times by progressively reducing centre distance at each repetition (pass) to generate the desired rotor profile. The tool has N identical inserts with the profile described by a collection of points, $P_t(u_t, v_t)$, defined in the rotating $U_t V_t Z_t$ coordinate system. This frame is identical to $X_t Y_t Z_t$ when the insert's tip is on the $X_t Y_t$ plane, but rotates around Z_t-axis at the tool's rotation

speed. The profile of the insert used in this work is shown in Figure 3.1 (c). The profile of the groove machined after each pass is defined by the collection of $P_r(u_r, v_r)$ points defined in the $U_rV_rZ_r$ coordinate system, which is identical to $X_rY_rZ_r$ when the tool and rotor are in contact at the rotor's end plane and rotates around Z_r-axis at the rotor's rotation speed. The finished profile of the rotor used in this work is shown in Fig,3.1 (d).

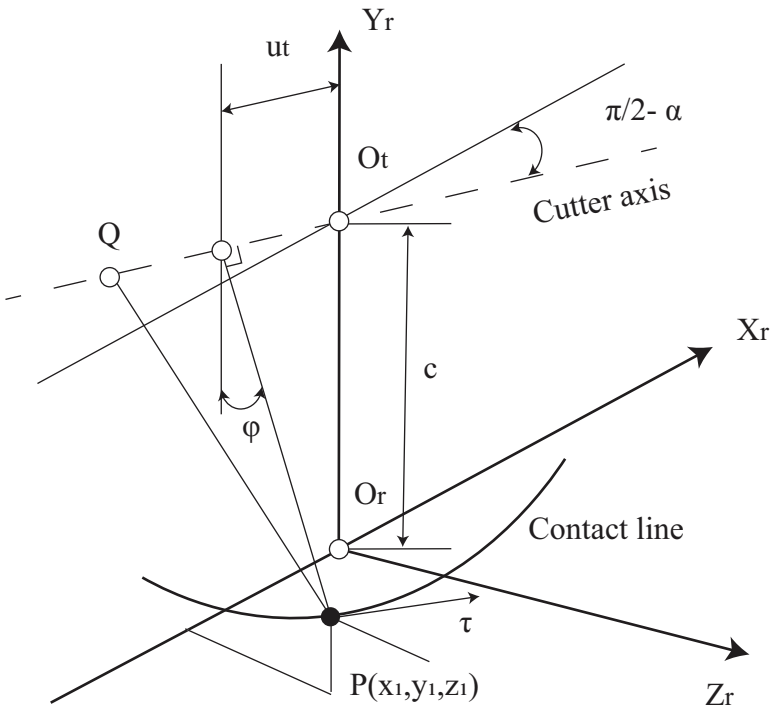

Figure 3.2: Illustration of Guo and Tang's kinematic model [11]

The kinematic model in Fig. 3.2 was presented by Guo and Tang to relate each tool profile point $P_t(u_t, v_t)$ to the resulting rotor profile $P_r(u_r, v_r)$, as follows [11] :

$$\begin{aligned} u_r &= -x_1 \sin\phi + y_1 \cos\phi \\ v_r &= x_1 \cos\phi + y_1 \sin\phi \end{aligned} \tag{3.3}$$

where x_1, y_1 and z_1 are the coordinates of the point on the contact line in the rotor coordinate system and $\phi = 2\pi z_1/L$ is the rotation angle between U_rV_r and X_rY_r coordinate systems. The coordinates of the points on the contact line are expressed

as:

$$\begin{bmatrix} x_1 \\ y_1 \\ z_1 \end{bmatrix} = \begin{bmatrix} c - v_t \cos\varphi \\ v_t \sin\varphi \cos\alpha + u_t \sin\alpha \\ v_t \sin\varphi \sin\alpha - u_t \cos\alpha \end{bmatrix} \tag{3.4}$$

where φ is the immersion angle shown in Fig. 3.2 and it is the only unknown variable. To find the rotor profile $P_r(u_r, v_r)$, the immersion angle φ need to be solved. From Fig. 3.2, $\overline{QP}$ is the common normal vector of cutter envelope and rotor flute surface at contact point $P(x_1, y_1, z_1)$. It will always intersect with the cutter axis at Q since the cutter is a revolving surface. $\overline{QP}$ can be expressed in Equation 3.5.

$$\overline{QP} = \begin{bmatrix} -v_t \cos\varphi \\ v_t \sin\varphi \sin\alpha + v_t \dot{v}_t \cos\alpha \\ -v_t \sin\varphi \cos\alpha + v_t \dot{v}_t \sin\alpha \end{bmatrix} \tag{3.5}$$

The vector $\bar{\tau}$ is on the contact line and in the direction along the rotor helical groove, expressed in Equation 3.6.

$$\begin{bmatrix} \tau_x \\ \tau_y \\ \tau_z \end{bmatrix} = \begin{bmatrix} -\left(\frac{2\pi}{L}\right) y_1 \\ \left(\frac{2\pi}{L}\right) x_1 \\ 1 \end{bmatrix} \tag{3.6}$$

Since the tool and the rotor surfaces are tangent to each other on the contact point $P(x_1, y_1, z_1)$, the contact line is established based on the orthogonality between the vector $\overline{QP}$ and the vector $\bar{\tau}$.

$$\overline{QP} \cdot \bar{\tau} = 0 \tag{3.7}$$

The variable φ is obtained by numerically solving the Equation 3.8 by substituting Equation 3.5 and Equation 3.6 into Equation 3.7.

$$\left(\frac{2\pi}{L}\right)(u_t + v_t \frac{dv_t}{du_t}) \sin\alpha \cos\varphi + \left(\frac{2\pi c}{L} \cos\alpha + \sin\alpha\right) \sin\varphi - \left(\frac{2\pi c}{L}\right)(\frac{dv_t}{du_t} \sin\alpha) + \frac{dv_t}{du_t} \cos\alpha = 0 \tag{3.8}$$

3.1 Example

In this section, Guo and Tang's kinematic model, described in Eqs. 3.3 to 3.8, is used to determine the profile of a rotor machined by a given insert profile mounted at a specific setup angle and center distance. The computed profile is then compared to the one generated by MACHpro, a dexel-based virtual machining software. The insert profile, shown in Fig. 3.3, is defined by 1000 points for the kinematic model and by 30 points for the dexel-based model. Fewer points had to be used for the dexel-based model to achieve a reasonable computation time, but a high number of points can be used in the kinematic model because its computation time is short. The machining process consists of five roughing passes and a finishing pass. The geometrical parameters of the cutter and rotor as well as the machining parameters in each of the six passes are shown in Table 3.1.

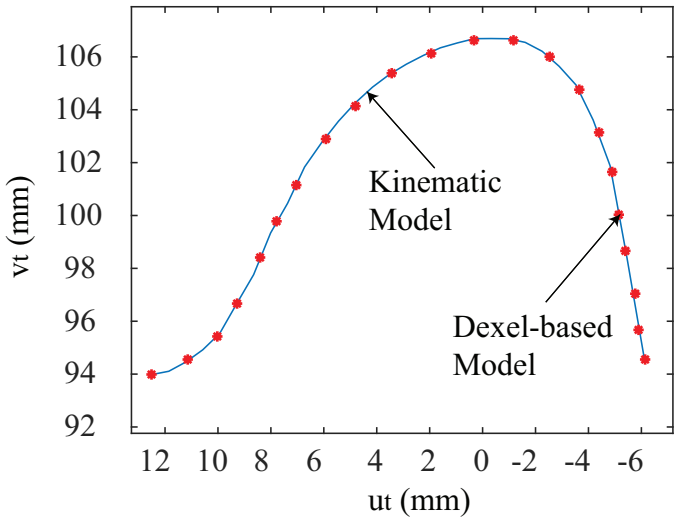

Figure 3.3: Insert profile defined by discrete points for the kinematic model and dexel-based model

Machining Pass	Center Distance c [mm]	Linear Velocity V_l [mm/s]	Spindle Speed ω_c [rad/s]	Rotor Rotation Speed ω_r [rad/s]
Roughing 1	134.1679	14.8167	45.5531	0.3773
Roughing 2	132.1156	14.8167	45.5531	0.3773
Roughing 3	130.2233	14.8167	45.5531	0.3773
Roughing 4	128.0795	14.8167	45.5531	0.3773
Roughing 5	126.0780	14.8167	45.5531	0.3773
Finishing	125.3744	3.4713	39.2699	0.0884
	Cutter Radius R_t [mm]	Inserts Number N	Rotor Radius R_r [mm]	Rotor Length $L_r[mm]$
Constant	106.6800	16	32.2580	115.6500
Parameters	Rotor Helix Angle θ [degrees]	Lead Distance L [mm]	Setup Angle α [degrees]	
	50.5991	188.6281	50	

Table 3.1: Geometrical and Machining Parameters

The resulting rotor profile can be computed directly with the kinematic model, but considerable post-processing is required to obtain the profile with the dexel-based method. First, a multi-axis Cutter Location (CL) file is generated to describe the combination of the relative linear and rotary motions between the tool and the rotor. The process is then simulated in the dexel-based software to generate the 3D model of the machined rotor in STL format. The triangle vertices that contribute to the 2D cross-section of the rotor are then identified and used to describe the resulting rotor profile. The resulting rotor profiles after each one of the six passes computed by the kinematics methods are shown in Fig. 3.4(d). Part (a-c) of the same figure shows the comparison of the final rotor profile (after finishing pass) computed by the kinematics method and the dexel-based method. Both of the methods generate similar profiles with negligible deviations caused by the lower resolution of the dexel-based model and loss of precision while extracting data from the CAD model in STL format.

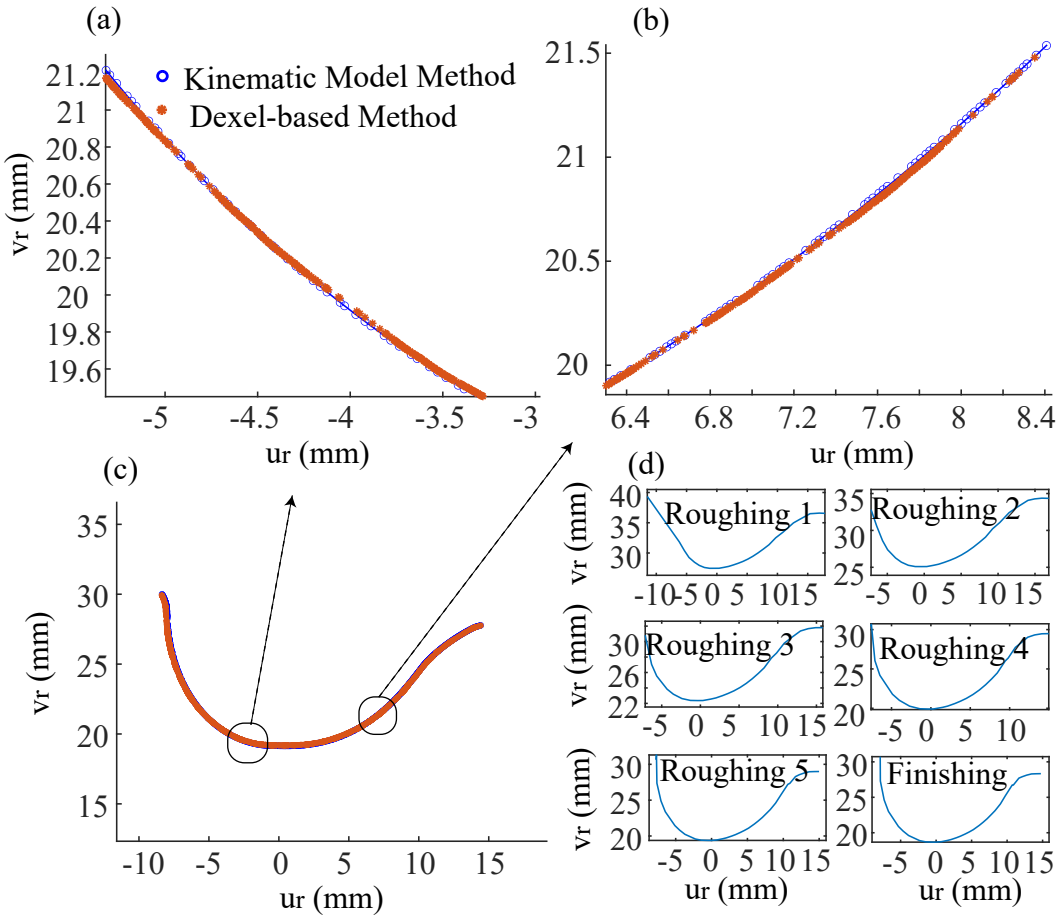

Figure 3.4: Comparison of the machined profile obtained from the kinematic model and dexel-based simulations

Deviations in the machining setup parameters such as setup angle and center distance can cause significant errors in the rotor profile. The higher computational efficiency of the kinematic model enables studying the sensitivity of the rotor profile to such deviations. Figures 3.6(a) to 3.6(d) show the effect of four types of setup misalignment on the profile error, which are the setup angle, center distance, tool position in X_t coordinate and the pivot angle. The studied misalignment types are defined in Fig. 3.5. The setup angle and pivot angle misalignment are normally contributed by rotor saddle and fixture. On the contrary, the center distance and tool position errors are mostly due to the cutter positions. It is observed that the profile deviations caused by the pivot angle and the tool position are similar to the rotor profile twisting around its center axis. After best fitting the deviated profiles caused by these two types of geometry errors to the nominal profiles, the final profile deviations are greatly diminished. However, this research considers the direct effects of

the manufacturing errors on the rotor profiles.

In each of Figs. 3.6(a) to 3.6(d), one misalignment type is varied in the model while the rest are kept constant at their nominal values. Deviations in setup angle and center distance are considered by simply using their deviated values instead of the nominal values in the model. The range of setup angle error is from -0.05 to 0.05 degrees. The range of pivot angle is from -0.2 to 0.2 degrees. Deviations in the X_t position are considered by shifting the u_t coordinate of the insert by the deviation value and then using the new insert profile in the model. Similarly, the deviation of the pivot angle is considered by rotating the nominal u_t and v_t coordinates of the insert by the deviation angle around the Z_t axis. The errors of the tool position in the X_t coordinate are between -0.508 to 0.508 mm and the center distance is between -0.015 to 0.015 mm. The values of undercut and overcut in all of the misalignment types are shown in the respective plots, except for center distance misalignment. Because positive and negative center distance deviations result in undercut and overcut, respectively, the maximum and minimum profile deviations are shown instead. The sensitivity analysis in the kinematic model agrees with the results from the dexel-based model.

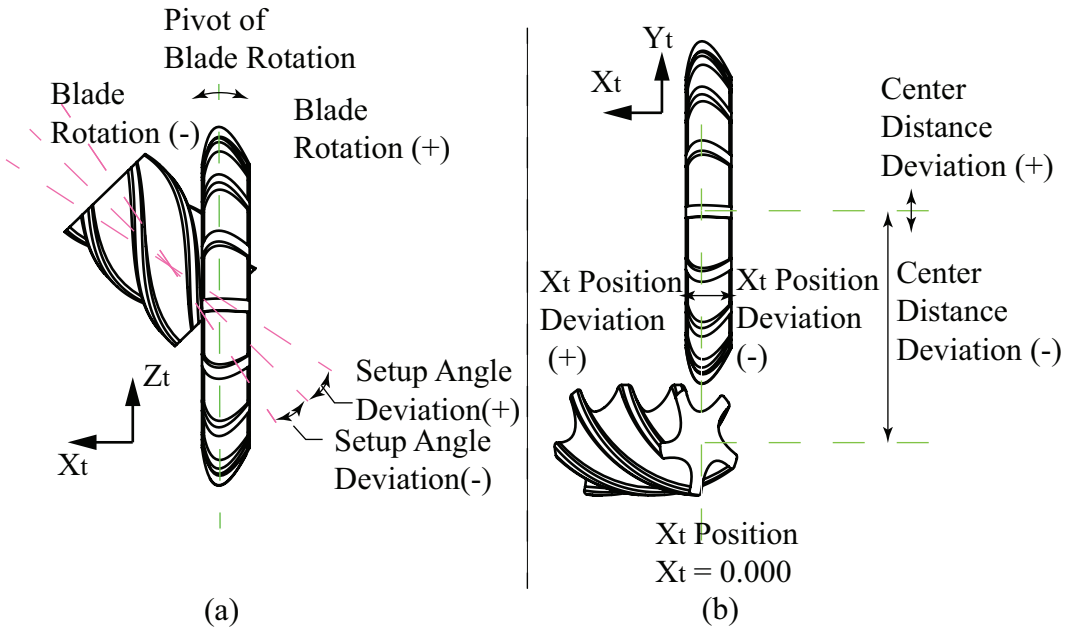

Figure 3.5: Potential misalignment between the tool and workpiece

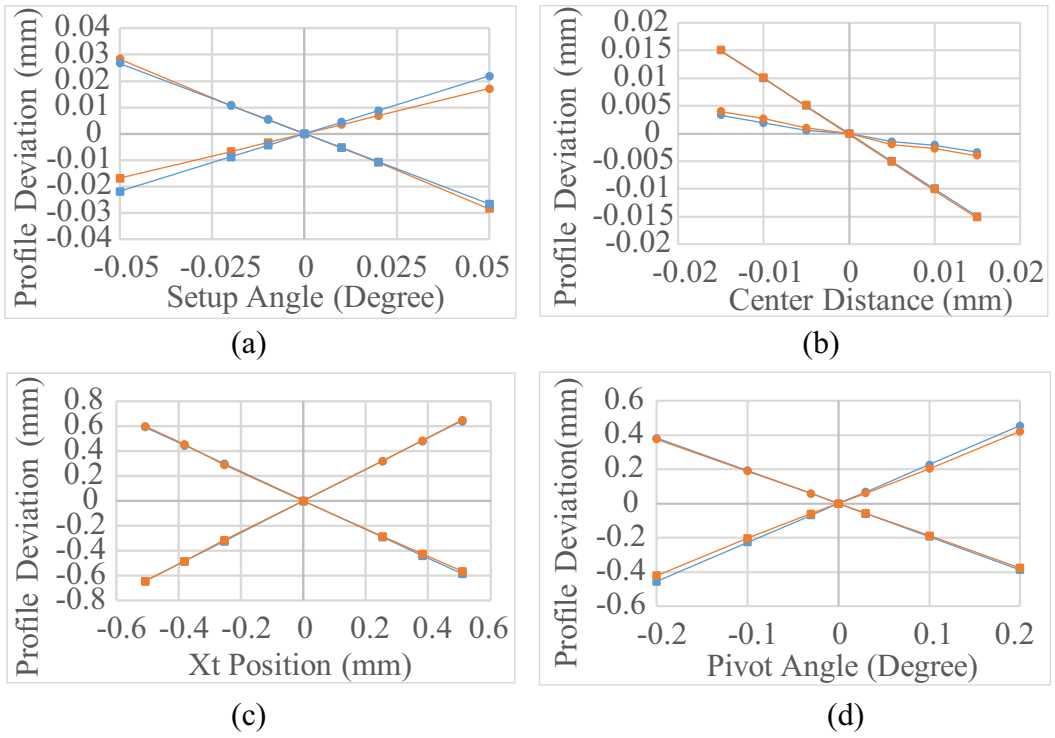

Figure 3.6: Sensitivity analysis for different types of misalignment

Chapter 4

Milling Forces

To simplify the milling force model derivations, and considering the typically small radial immersion in rotor milling processes, only one of the tool's inserts is assumed which is engaged with the workpiece at a time. Extension to rare cases where multiple inserts cut simultaneously is straightforward. Forces are computed at discrete time instants, $t_i = i\Delta t, i = 0, 1, ..., N_t$, where the time increment is denoted Δt. The instantaneous immersion angle of the cutting insert $\phi_i = \omega_c i\Delta t$ is measured from Y_t-axis, as shown in Fig. 4.1. The curved profile of the insert is divided into $k = 1, ...K$ points with each two consecutive points creating a straight cutting edge (or segment). The forces applied to each segment are computed in its local TRA coordinate frame shown in Fig. 4.1(b). The tangential axis, T, is in the direction of cutting speed. The unit vector in the tangential direction can be expressed as $\boldsymbol{e}_t(i) = [0 \quad -\sin\phi_i \quad \cos\phi_i]^T$ in the tool frame $(X_tY_tZ_t)$. The unit vector in the radial direction, R, is perpendicular to the cutting speed and cutting edge directions; the radial unit vector can therefore be expressed as $\boldsymbol{e}_r(i,k) = \boldsymbol{e}_t(i) \times \frac{\boldsymbol{l_k}}{||\boldsymbol{l_k}||}$, where $\boldsymbol{l_k}$ is the cutting edge vector, defined as follows in the tool frame:

$$\boldsymbol{l}_k = \begin{bmatrix} 1 & 0 & 0 \\ 0 & \cos\phi_i & -\sin\phi_i \\ 0 & \sin\phi_i & \cos\phi_i \end{bmatrix} \begin{Bmatrix} u_{tk} - u_{tk-1} \\ v_{tk} - v_{tk-1} \\ 0 \end{Bmatrix}; k = 2..K \tag{4.1}$$

The unit vector in axial direction (A) is obtained as the cross-product of the radial and tangential unit vectors, i.e. $\boldsymbol{e}_a(i,k) = \boldsymbol{e}_r(i,k) \times \boldsymbol{e}_t(i)$.

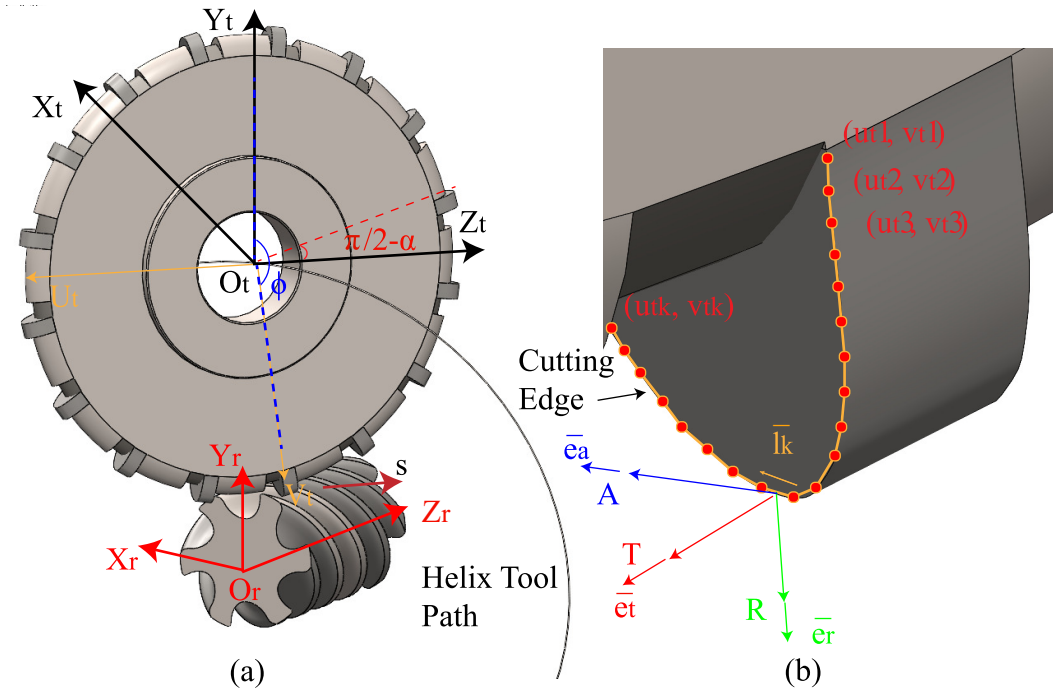

Figure 4.1: Local forces acting on the cutting edges

Linear mechanistic force model is used to describe the forces applied to each cutting segment:

$$\boldsymbol{f}_q(i,k) = ||\boldsymbol{l}(k)||\left(K_{qc}(k)h(k,i) + K_{qe}\right)\boldsymbol{e}_q(i,k); q = r,t,a \tag{4.2}$$

where K_{qc} and K_{qe}, $q = r,t,a$, are cutting and edge force coefficients in their respective directions. Chip thickness, $h(i,k)$, is determined by projecting the feed vector onto the radial direction ($\boldsymbol{e}_r(i,k)$):

$$h(i,k) = \boldsymbol{s}.\boldsymbol{e}_r(i,k) \tag{4.3}$$

Feed vector, $\boldsymbol{s}$, shown in Fig. 4.1(a), comprises linear and rotational components that are generated by the helical motion of the rotor. Components of this vector in the tool frame are expressed as follows:

$$\boldsymbol{s} = \begin{bmatrix} \sin\alpha & 0 & \cos\alpha \\ 0 & 1 & 0 \\ -\cos\alpha & 0 & \sin\alpha \end{bmatrix} \begin{Bmatrix} -(c-R_t)\omega_r\cos(\omega_r t) \\ -(c-R_t)\omega_r\sin(\omega_r t) \\ V_l \end{Bmatrix} \tag{4.4}$$

The vector of overall forces, $\boldsymbol{F}(i\Delta t)$, in the tool frame are obtained by summing the

forces applied to all of the segments that are engaged with material:

$$\boldsymbol{F}(i\Delta t) = \sum_{k=1}^{K} \sum_{r,t,a} \boldsymbol{f}_q(i,k) g(i,k) \tag{4.5}$$

and $g(i,k)$ is one if the corresponding segment (k) is engaged with the material and zero otherwise. The method presented in the next section is used to determine the engagement condition of the cutting edges (segments).

4.1 Cutter-Workpiece Engagement (CWE)

The engagement of each segment with the workpiece is determined by its position relative to the helical surface generated in the preceding (roughing) pass and the 3D surface swept by the preceding insert in the current pass. These two surfaces are denoted S_0 and S_1 in Fig. 4.2. All of the engaged segments (with $g(k,i) = 1$) are located below both of those surfaces, and the rest are not engaged with the material and thus no forces are applied to them ($g(k,i) = 0$).

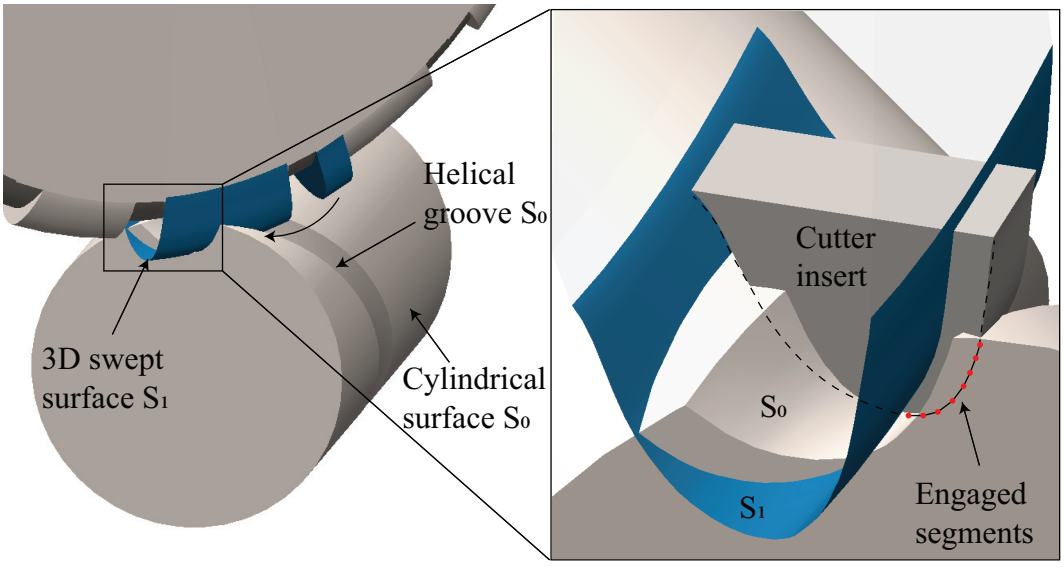

Figure 4.2: Surface boundaries. (a) machined surface and swept surface, (b) engaged segments under surface boundaries

Machined surface

At the beginning of the initial roughing process, the rotor surface is a cylinder. At the beginning of subsequent roughing passes, the rotor's surface is a combination of the cylindrical surface and helical grooves machined in the preceding roughing pass, shown in Fig. 4.2 (a). The cross sections of the existing helical groove corresponding with the Z_r-coordinates of the two ends of each segment were used to determine whether that segment is below the S_0 surface. The coordinates of the two ends of the segment in the rotor coordinate system ($X_rY_rZ_r$) are obtained as follows:

$$\begin{Bmatrix} x_{rk} \\ y_{rk} \\ z_{rk} \end{Bmatrix} = \begin{bmatrix} \sin\alpha & 0 & -\cos\alpha \\ 0 & 1 & 0 \\ \cos\alpha & 0 & \sin\alpha \end{bmatrix} \begin{bmatrix} 1 & 0 & 0 \\ 0 & \cos\phi_i & -\sin\phi_i \\ 0 & \sin\phi_i & \cos\phi_i \end{bmatrix} \begin{Bmatrix} u_{tk} \\ v_{tk} \\ 0 \end{Bmatrix} + \begin{Bmatrix} 0 \\ c \\ 0 \end{Bmatrix}; \quad k = 1..K \quad (4.6)$$

The profile of the corresponding rotor cross-section is obtained after rotating the profile computed in Section 3 by $2\pi z_{rk}/L$ radians around Z_r axis:

$$\begin{Bmatrix} x_{rj} \\ y_{rj} \\ z_{rj} \end{Bmatrix} = \begin{bmatrix} \cos\frac{2\pi z_{rk}}{L} & -\sin\frac{2\pi z_{rk}}{L} & 0 \\ \sin\frac{2\pi z_{rk}}{L} & \cos\frac{2\pi z_{rk}}{L} & 0 \\ 0 & 0 & 1 \end{bmatrix} \begin{Bmatrix} u_{rj} \\ v_{rj} \\ 0 \end{Bmatrix}; j = 1, 2, .. \quad (4.7)$$

If the y_{rk} coordinates of the two ends of the segment are smaller than the y_{rj} coordinate of the closest point to them, that segment is considered below the surface of the un-machined rotor; otherwise, it is considered above it.

At the first pass, the cross-section of the cylindrical surface is used to determined whether a segment is below the S_0 surface. The Y_r-coordinates of the circular cross-section corresponding with the X_r-coordinates of the two ends of each segment are determined as $\sqrt{R_r^2 - x_{rk}^2}$. If the y_{rk} coordinates of the two ends of the segment are smaller than $\sqrt{R_r^2 - x_{rk}^2}$, that segment is considered below the surface of the un-machined rotor; otherwise, it is considered above it.

Swept surface

The surface swept by the cutting insert is approximated by the ensemble of 2D insert profiles rotated at $\omega_c \Delta t$ increments about the tool's axis. In the subsequent

tooth-passing period, this surface will have moved along the rotor's helical trajectory, however, considering the typically short tooth passing periods, the motion along the helix can be approximated by a linear motion parallel to X_rZ_r plane. As a result, the ensemble of the insert profiles that defines the swept surface can be obtained as follows in the rotor coordinate system:

$$\begin{Bmatrix} x_{ik} \\ y_{ik} \\ z_{ik} \end{Bmatrix} = \begin{bmatrix} \sin\alpha & 0 & -\cos\alpha \\ 0 & 1 & 0 \\ \cos\alpha & 0 & \sin\alpha \end{bmatrix} \left(\begin{bmatrix} 1 & 0 & 0 \\ 0 & \cos(\omega_c i\Delta t) & -\sin(\omega_c i\Delta t) \\ 0 & \sin(\omega_c i\Delta t) & \cos(\omega_c i\Delta t) \end{bmatrix} \begin{Bmatrix} u_{tk} \\ v_{tk} \\ 0 \end{Bmatrix} + \begin{Bmatrix} \frac{-s_x 2\pi}{N\omega_c} \\ c \\ \frac{-s_z 2\pi}{N\omega_c} \end{Bmatrix} \right); k = 1..K, i = 0..\frac{2\pi}{N\Delta t\omega_c}; \quad (4.8)$$

If the y_{rk} coordinates of the two ends of the segment (in Eq. 4.6) are smaller than the y_{ik} coordinate of the closest point to them, that segment is considered below the swept surface; if not, it is considered above it.

4.2 Example

The presented force model is used to simulate the forces in milling the rotor described in Chapter 3.1 and the results are validated by comparing them against the forces simulated by a dexel-based software, MACHPRO™ [29]. The insert profile was defined by K=30 points as shown in the Fig. 3.3. The cutting coefficients of AISI 1045 Steel workpiece are determined from orthogonal cutting database at $K_{tc} = 1662$, $K_{rc} = 597$, and $K_{ac} = 157$ MPa [30]. The edge coefficients K_{qe} are assumed zeros.

The machining process comprises five roughing passes and one final finishing pass. The machining parameters in each pass are shown in Table 3.1. Simulation time-step Δt=0.001 seconds was used to compute the forces in each of the six passes and the resulting forces are shown in Figs. 4.3 to 4.5. Also shown in those figures are the forces simulated by the dexel-based software. To keep the computation time of the dexel-based method manageable, a larger simulation time-increments of 0.018 seconds was used. As a result, only the envelope of the force signals are obtained from this method, whereas the much higher computational efficiency of the presented method allows for simulating the force variation during each tooth-passing period. The forces

simulated by both of the methods are consistent for all of the roughing passes. Forces during the last finishing pass deviate in two methods. The CWE geometry in the finishing pass is much smaller than the roughing pass, and therefore more affected by the course resolution of the dexel-based simulation and simplifying assumptions made in the kinematic approach. Consequently, the simulated finishing forces deviate in the two methods.

In the kinematic model, the chip thickness is found by projecting the feedrate to the radial vectors on each of the cutting edge segments. Since the radial vectors are changing along the cutting edges, the chip thickness will also vary for different cutting edge segments. Fig. 4.6 shows the maximum chip thickness generated among all the cutting edge segments which engage the workpiece at any time instance. The variation of the chip thickness for each tooth passing period agrees with the cutting forces results.

Fig. 4.7 compares the force simulation time in the dexel-based software and kinematic model. The simulation time step is in the range of 0.05 - 0.02 seconds. In the dexel-based software, the simulation time increased extremely fast as the simulation time step becomes finer. And the simulation time raised dramatically when the time step smaller than 0.025 seconds. In the kinematic model, however, the simulation time grew slowly and is always less than 1 minute as the time step becomes smaller.

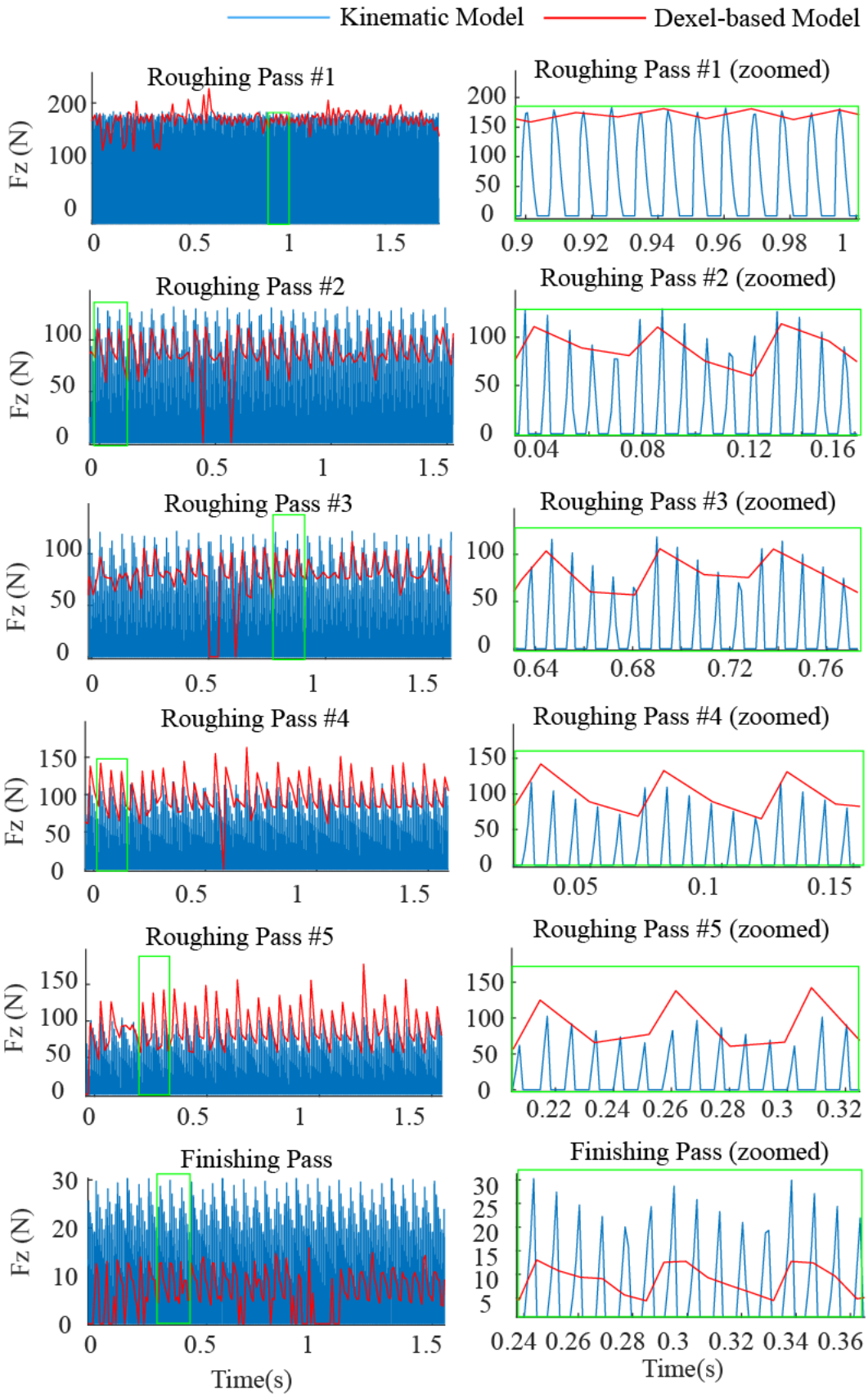

Figure 4.3: Overall forces in Z_t axis

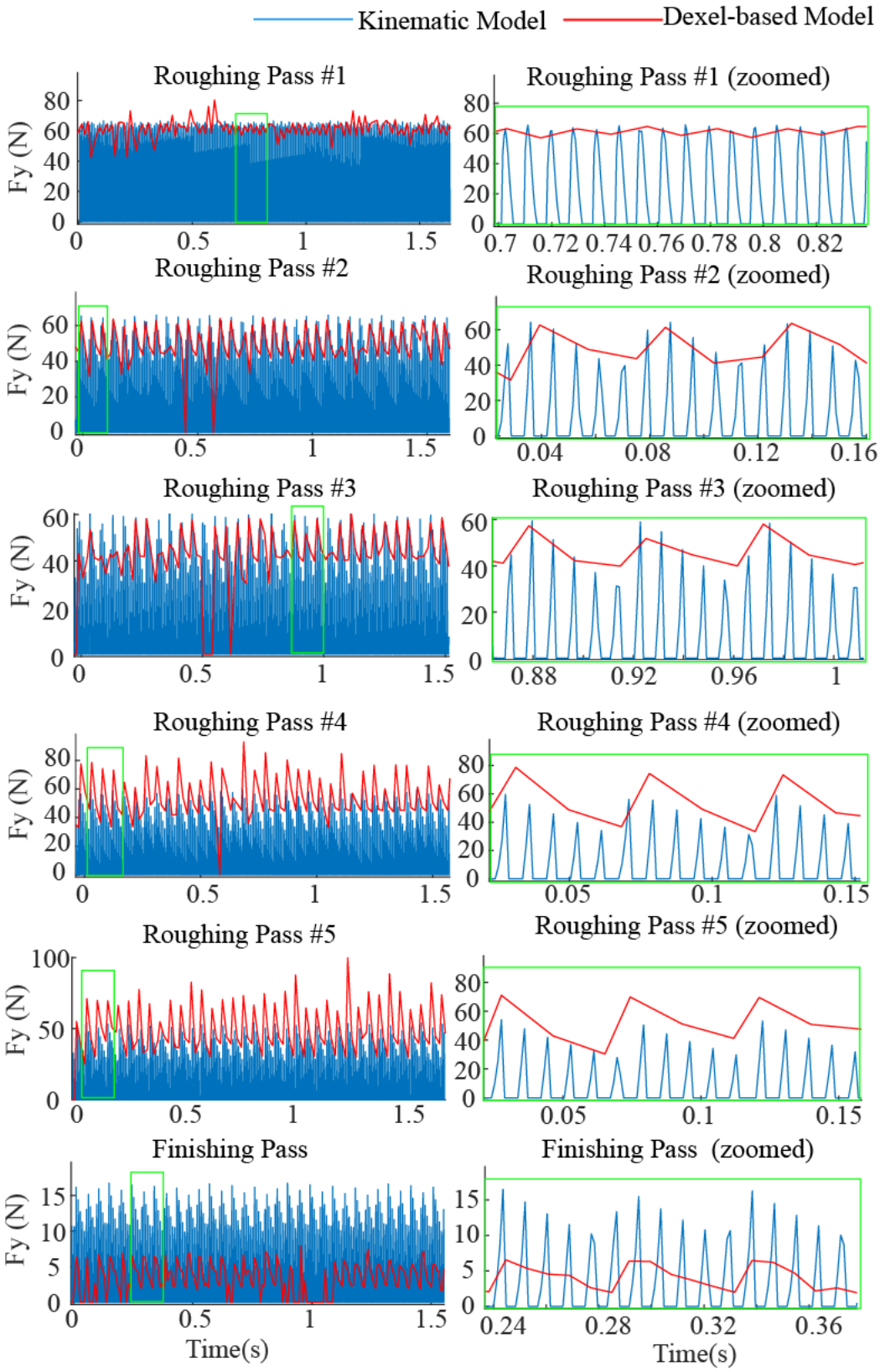

Figure 4.4: Overall forces in Y_t Axis

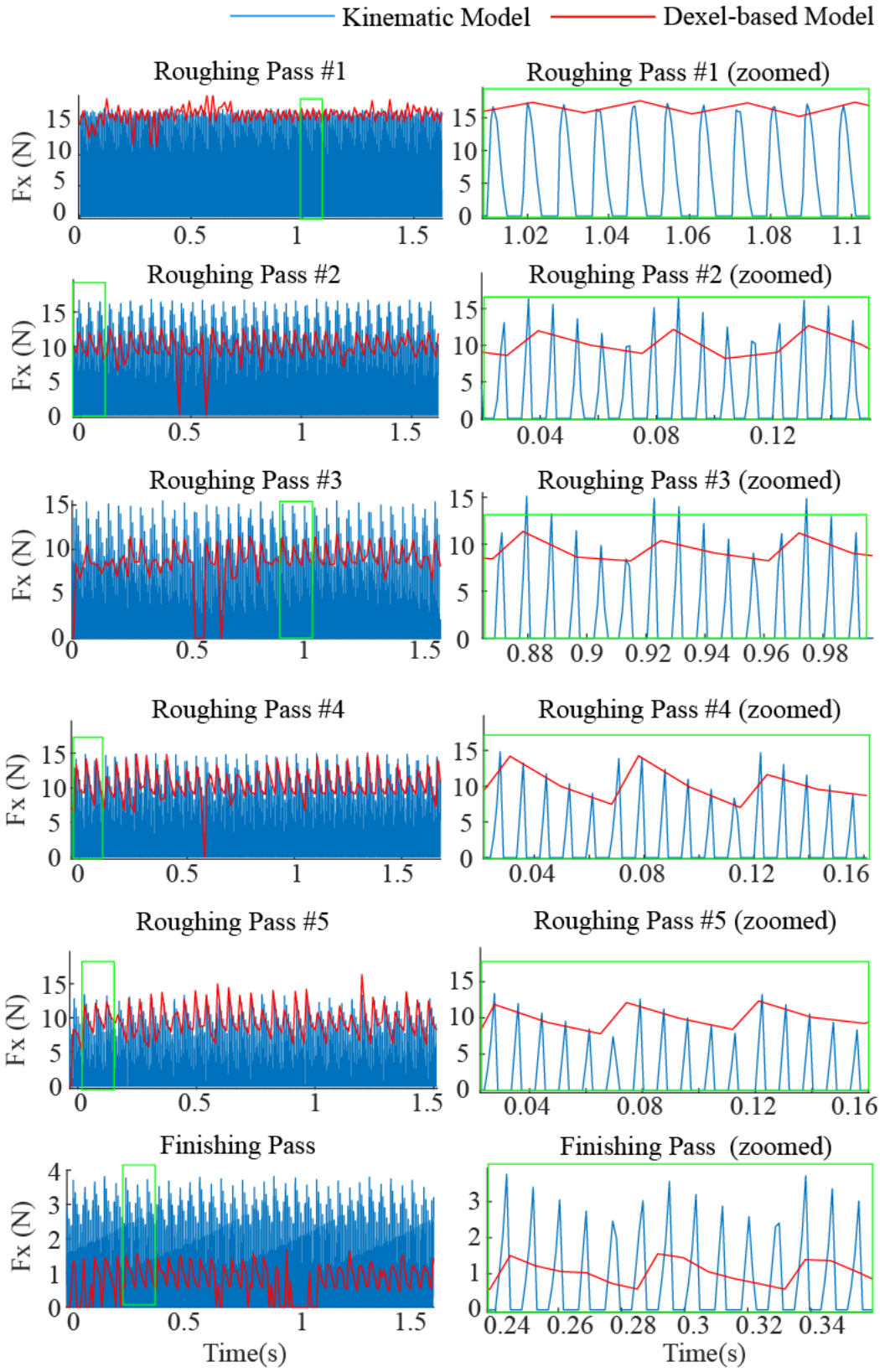

Figure 4.5: Overall forces in X_t Axis

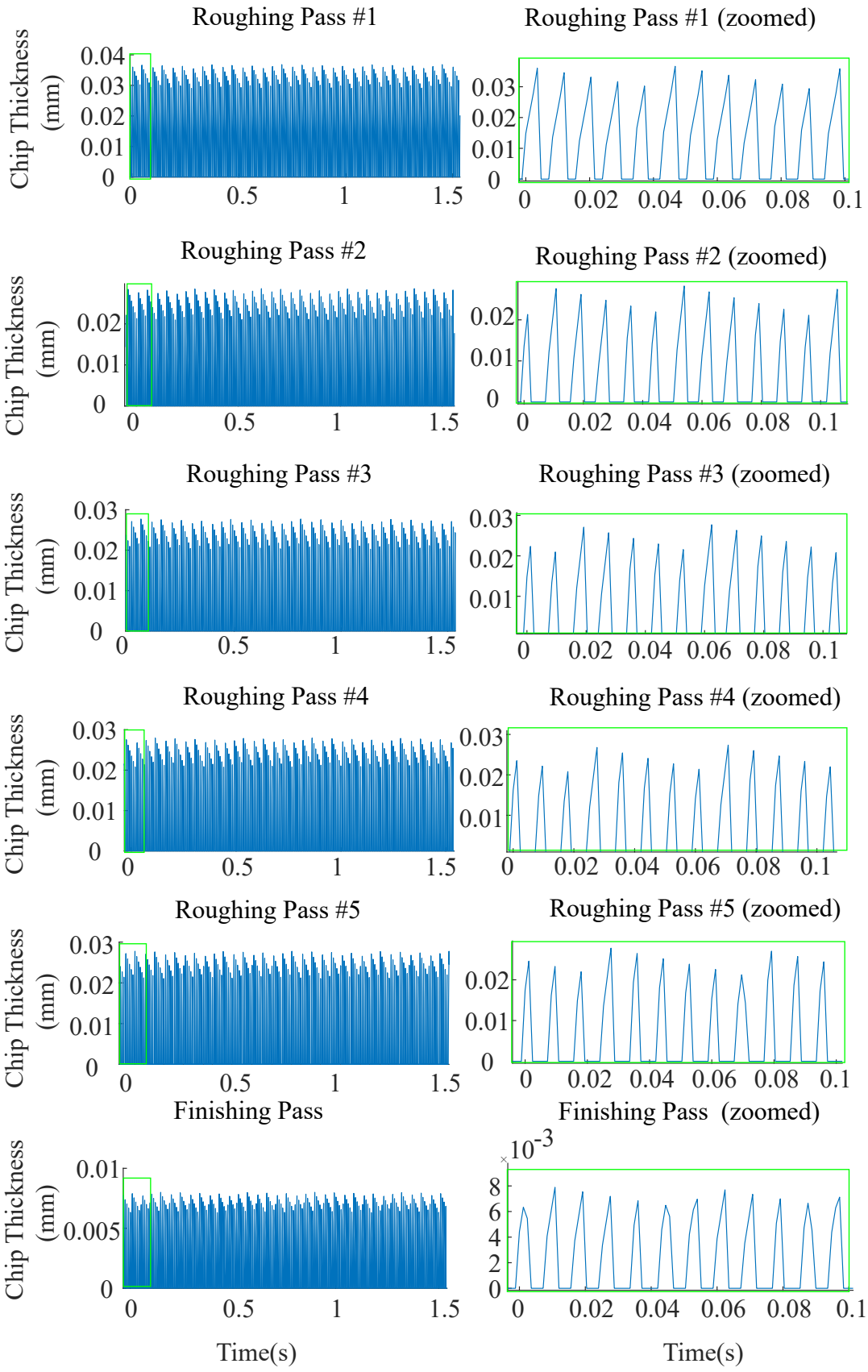

Figure 4.6: Maximum chip thickness

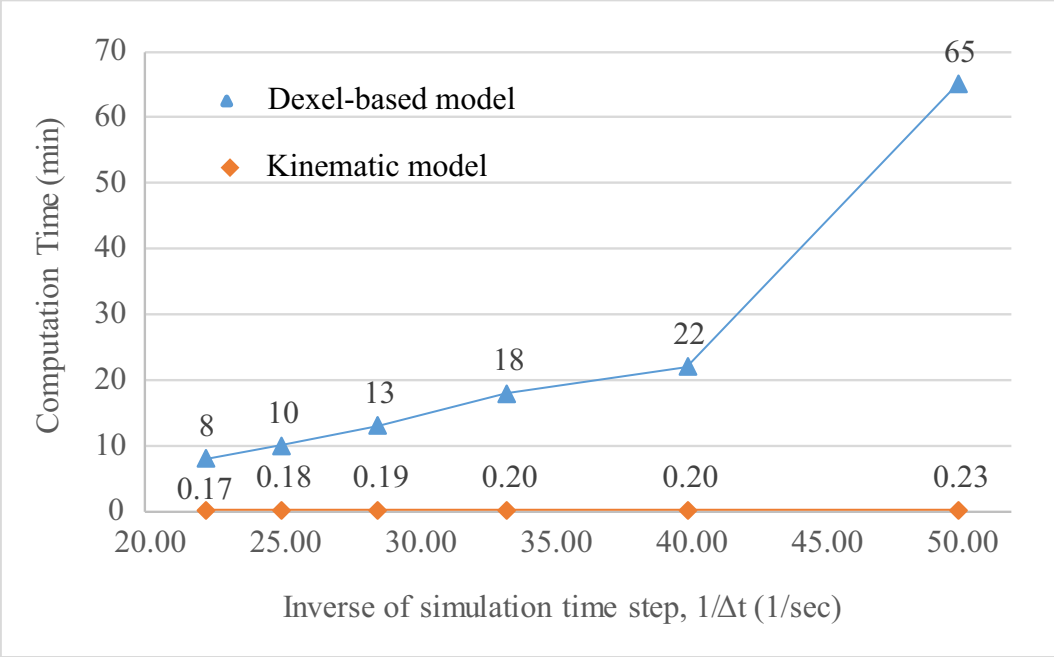

Figure 4.7: Comparison of the simulation time from the kinematic model and dexel-based model

Chapter 5

Conclusion and Future Work

A new method was presented to simulate the forces in milling screw-rotors. Because the CWE are obtained semi-analytically based on the kinematics model of the process, and not computationally intensive graphical simulations, the presented method can simulate the forces with arbitrary resolution in a reasonable time.

A comparison of the forces simulated by the presented method and a dexel-based virtual machining software verified their accuracy. In the presented examples, the resolution of force simulation in the dexel-based method had to be reduced substantially to achieve a manageable simulation time (approximately 82 minutes). The computation time for the same example with 18 times higher time resolution was only 15 minutes. The short computation time of the presented method enables its use in optimization algorithms where the machining parameters are adjusted to reduce forces and the resulting deviations in the rotor profile.

Dynamic analysis such as cutter vibrations and stability lobe diagram is the future work for this developed kinematic model. However, the tool deflections can be predicted using a numerical method by running a FEM simulation in SOLIDWORKS. As shown in Fig. 5.1 (a), the whole tool assembly is simplified into three main components: the spindle, the adapter and the cutter. Alloy steel is the material assigned in the spindle, carbon steel is assigned in both adapter and the cutter body, and the cutter inserts are assigned to AISI M2 steel. The FEM simulation setup is illustrated in Figure 5.1 (b). According to the results found in Chapter 4.2, the maximum milling forces in each pass are applied on the engaged inserts in tool coordinate $X_tY_tZ_t$ shown in Table 5.1. Figs. 5.2 to 5.4 show the tool deflection results in Z_t, Y_t, and X_t axis.

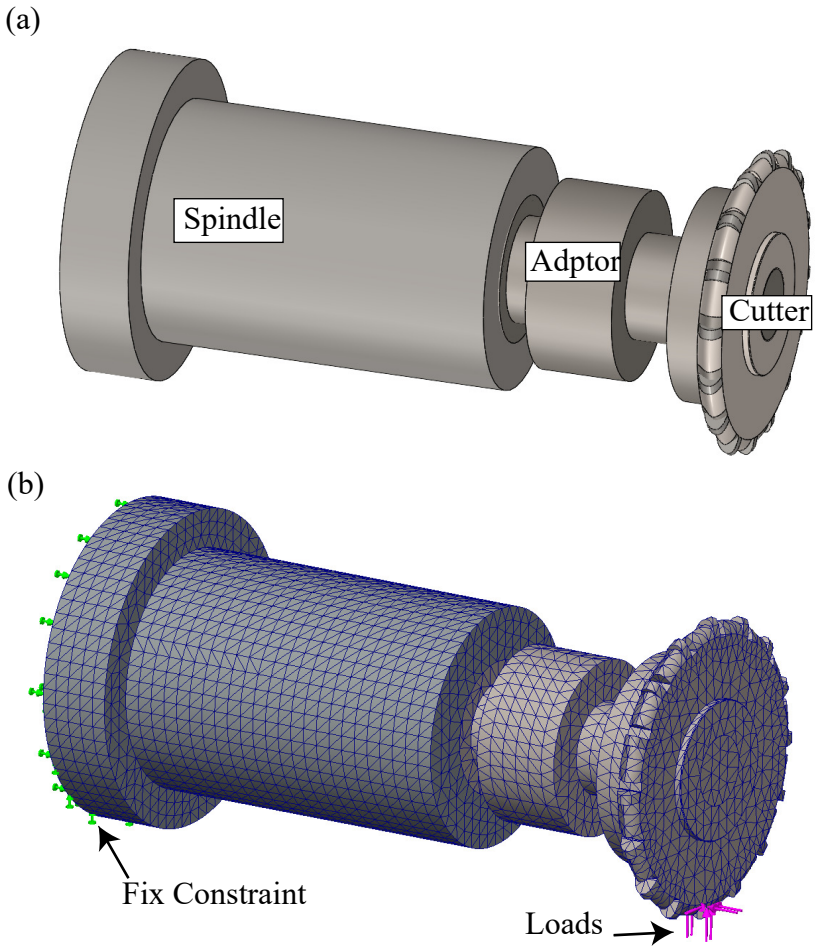

Figure 5.1: Tool FEM Assembly

Machining Pass	Feed Force F_z [N]	Normal Force F_y [N]	Axial Force F_x [N]
Roughing 1	238.9109	130.5135	31.1101
Roughing 2	132.1490	65.8735	16.8428
Roughing 3	121.4787	61.1375	15.4716
Roughing 4	117.1293	60.1056	14.9269
Roughing 5	105.3076	54.1114	13.3807
Finishing	30.6266	16.7146	3.8114

Table 5.1: Maximum Cutting Forces in each pass

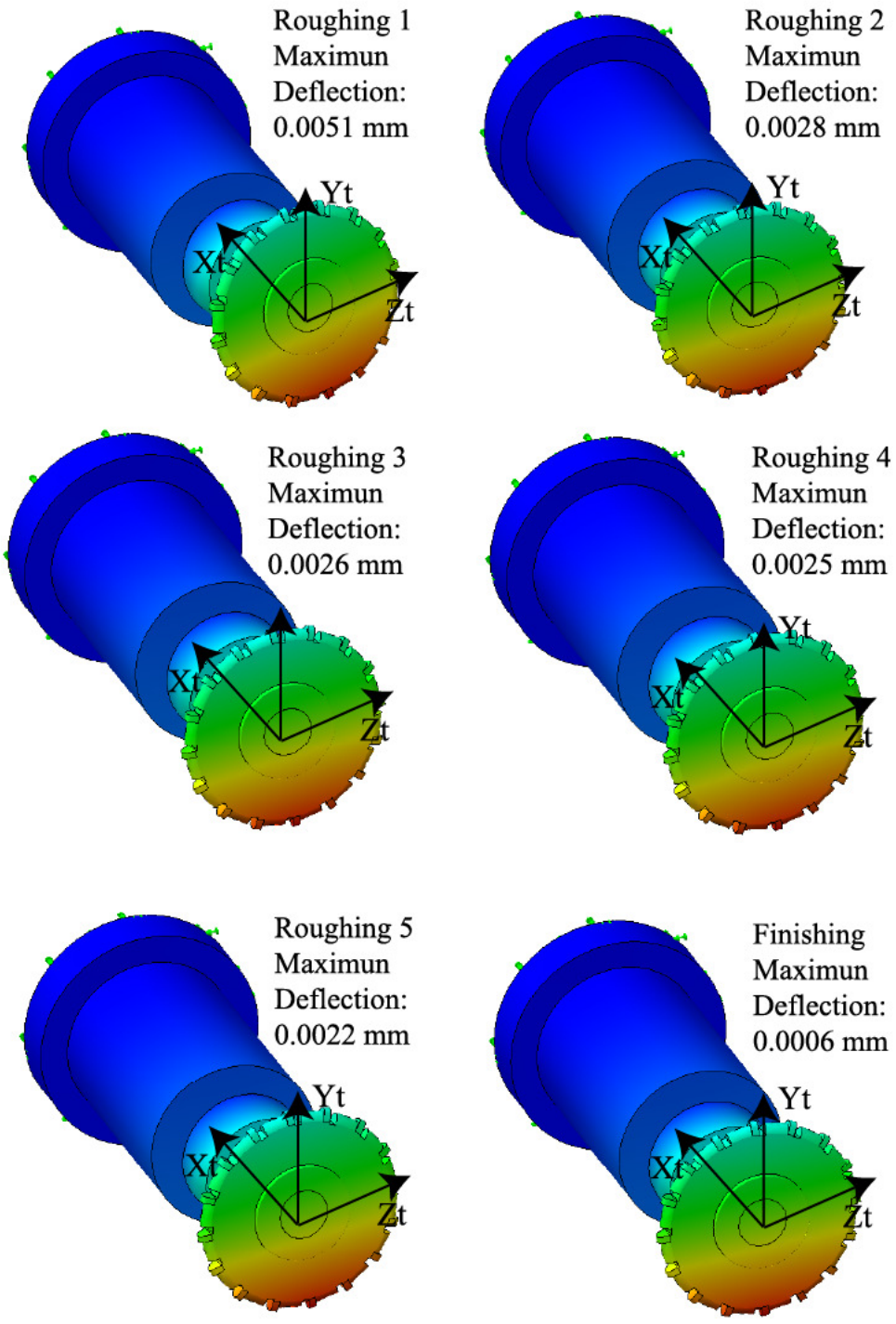

Figure 5.2: Maximum tool deflections in Z_t axis

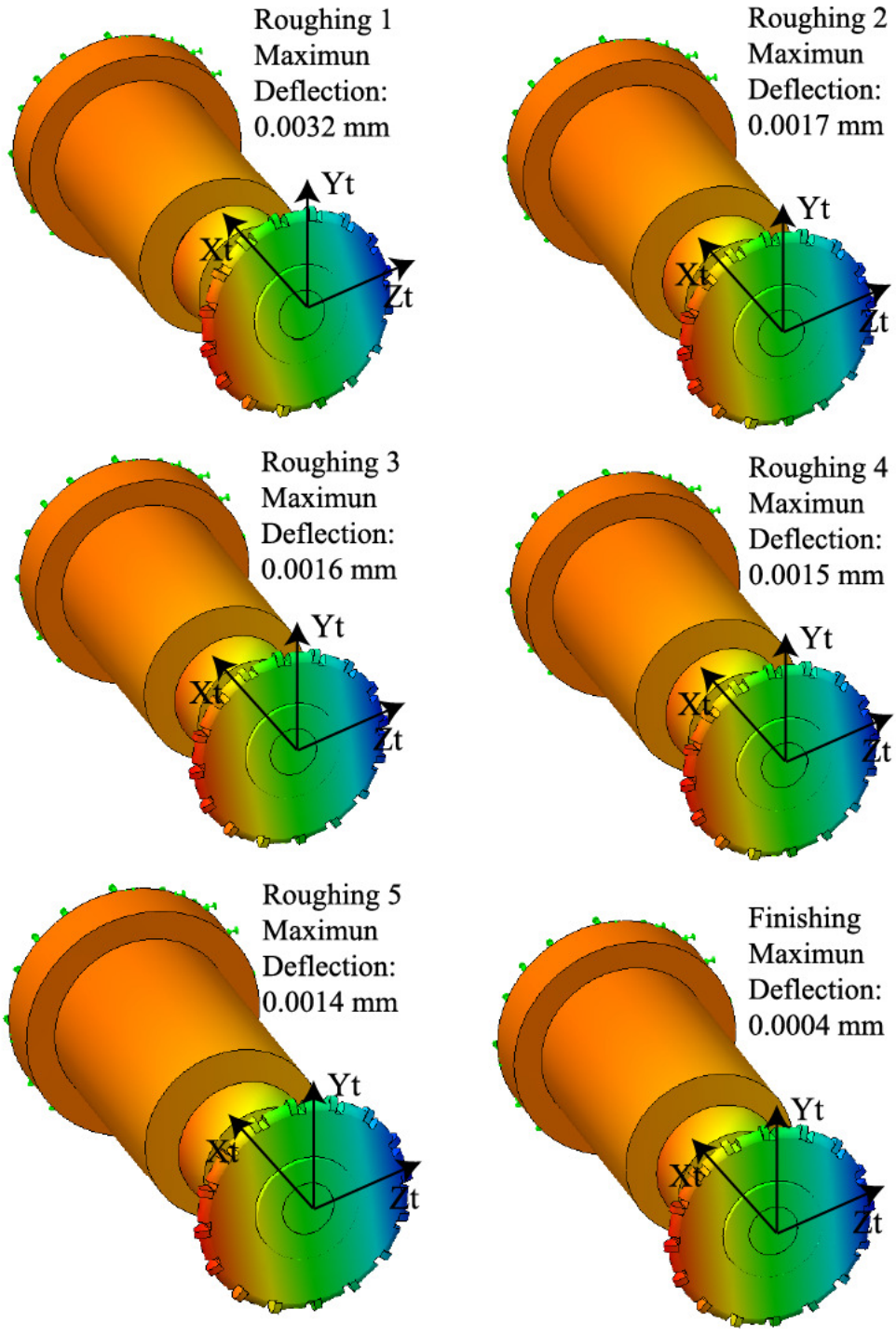

Figure 5.3: Maximum tool deflections in Y_t axis

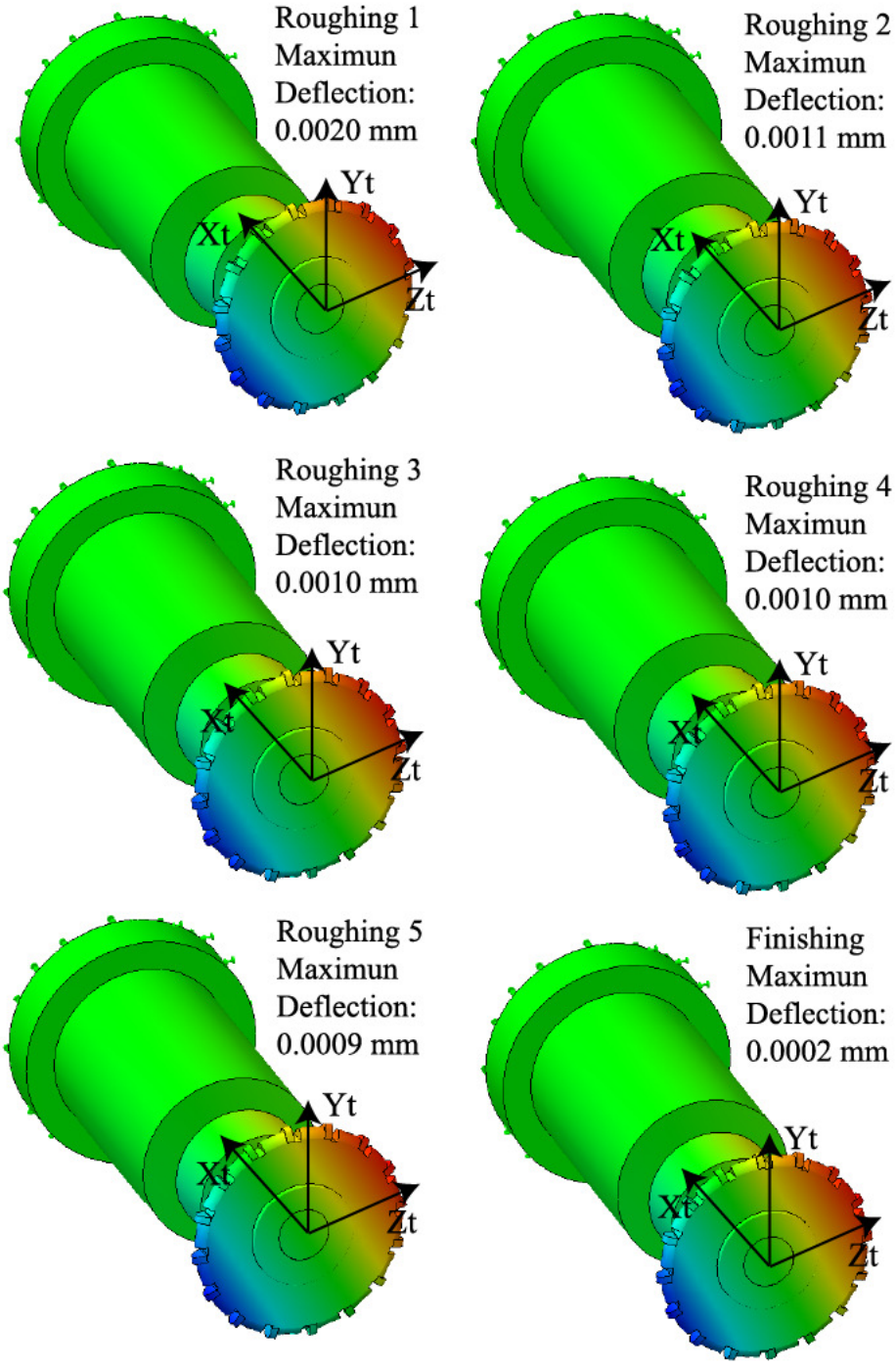

Figure 5.4: Maximum tool deflections in X_t axis

Table 5.2 shows the cutter maximum deflections in the tool coordinate system in each pass. Roughing processes, especially the initial roughing, contribute relatively

large deformations compared with the finishing process. However, the deformation in the finishing process is more important because it will directly affect the shape of the final rotor profile. The optimization in the finishing pass to reduce the cutter deflections is beneficial to increase the rotor profile accuracy during manufacturing.

Machining Pass	Maximum Deflection in F_z [mm]	Maximum Deflection in F_y [mm]	Maximum Deflection in F_x [mm]
Roughing 1	0.0051	0.0032	0.0020
Roughing 2	0.0028	0.0017	0.0011
Roughing 3	0.0026	0.0016	0.0010
Roughing 4	0.0025	0.0015	0.0010
Roughing 5	0.0022	0.0014	0.0009
Finishing	0.0006	0.0004	0.0002

Table 5.2: Cutter maximum deflection in the tool coordinate system

Appendix A

Specifications in Dexel-based Method

MACHpro is a dexel-based VMS software for process simulation and optimization. It is available to generate visualized geometry simulations and solve the physics within the machining operations. However, there are gaps to model the screw milling process in this graphical-based environment directly. One challenge is the workpiece has to be fixed during the simulation. It is solved by using the helical cutting kinematic [10] which is generated by combining the relative linear and rotary motions and saved in the CL file. Another challenge is the software restricts uploading negative profile points to generate the virtual cutter model. It can be overcome by adding composition distance into the helical tool path. In this appendix, the detailed setup procedures are shown to generate the rotor profiles and calculate the cutting forces.

A.1 Profile Prediction

The entire simulation setup in this dexel-based VMS is constructed by the specifications of the machining center, workpiece, tool, Cutter Location (CL) file and engagement distance. The virtual screw rotor milling process is performed on Haas VF-5 milling center. The workpiece is a dexel-based cylindrical model with radius of 32.2580 mm and length of 76.2 mm. The specified material for the workpiece is AISI 1045 Steel. The cutting force coefficients are $K_{tc} = 1662$, $K_{rc} = 597$, $K_{ac} = 157$ MPa and edge force coefficients K_{qe} are zeros. The cutter model is generated by revolving the 30 discretized profile points shown in Fig. 3.3 around its center axis.

The flute number is 16 with zero degree flute angle. CL file describes the cutter's space and angular positions along the helical tool path and specified the cutter's spindle speed and feedrate corresponding to the Table 3.1. In this work, each machining pass (roughing or finishing) cuts one groove on the rotor only, shown as Fig. A.1 (a). The computation interval for generating CWE maps, which is called the engagement maps sampling distance, is specified as 1 mm. It can be observed that, various approaches are used to reduce the simulation time, such as shorten the length of the rotor, decrease the cutter profile points, reduce the number of grooves on the rotor and increase the calculation interval. Fig. A.1 shows the virtual tool and workpiece created in MACHpro.

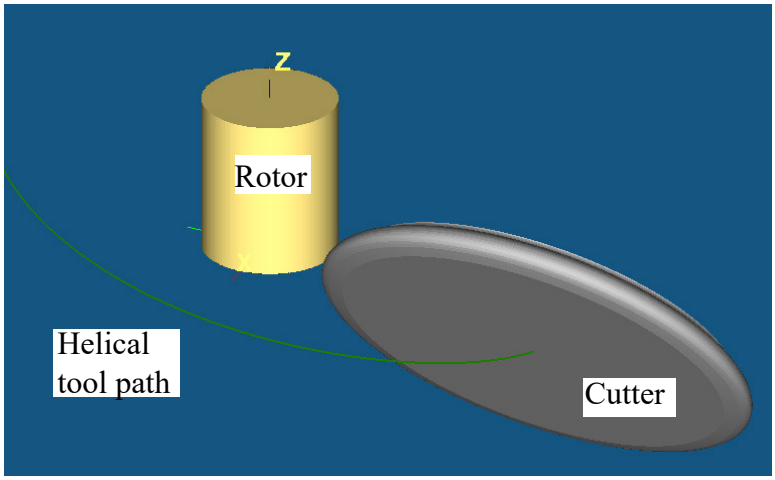

Figure A.1: Screw milling process in the dexel-based method

The machined rotor 3D model can be exported in Standard Tessellation Language (STL) format and the CWE maps are generated when the software simulation finished. To find the rotor profile from this STL model, it is sent to SOLIDWORKS and converted into a meshed body. The valid profile is any cross-sections perpendicular to the rotor axis. To plot the cross-section profile from the meshed body and compare it with the profile obtained in the kinematic-based method, the cross-section points are subtracted into the Excel spreadsheet. Based on the position of the cross-section along the rotor axis, the rotor profile angular position varies. To compare the predicted rotor profile from the kinematic model and the dexel-based model, the best fit method is required to transfer these two profiles in the same angular position. Fig. A.2 shows the procedures to obtain the profile points from the output STL model.

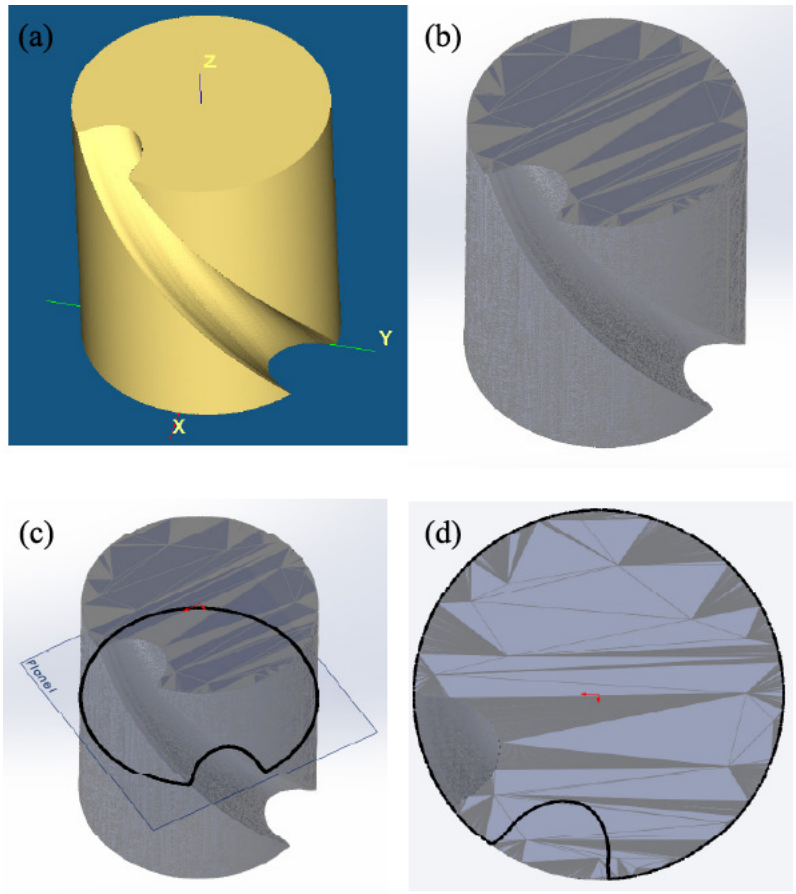

Figure A.2: Post processes in CAD software. (a). exporting the rotor model in STL format, (b). converting the rotor model in meshed solid body, (c). finding the cross-section perpendicular to the rotor axis, (d). transferring the data points of groove feature to spreadsheet

A.2 Forces Simulation

Based on the generated CWE, the maximum cutting forces at each discretized time segment are predicted using the average cutting force model in the tool coordinate system shown in Fig. A.3 (a). This dexel-based software uses a similar physics approach to find the global cutting forces by summing up the local forces on the discretized cutting edge segments. Fig. A.3 (b) shows the monitored CWE area on the tool in blue. This 3D contact area agrees with the CWE found in the kinematic model.

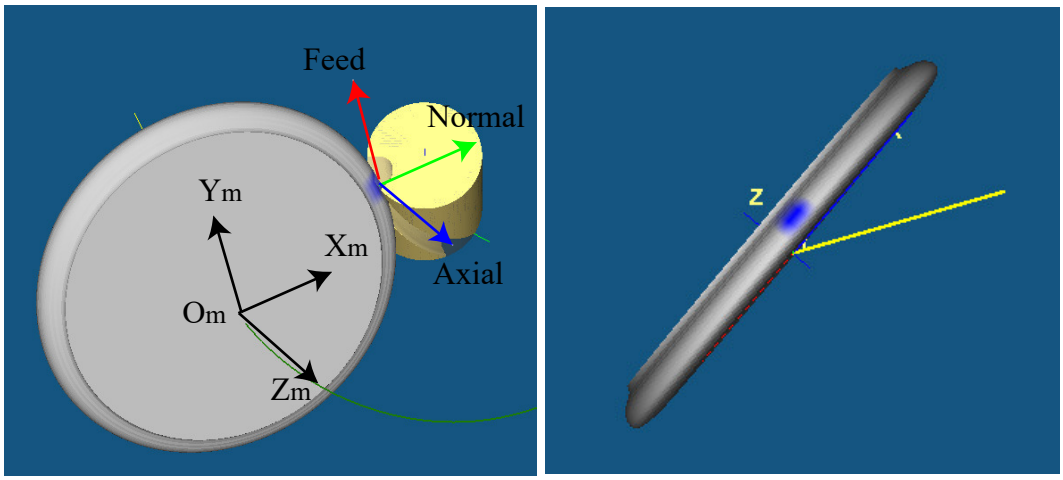

Figure A.3: Cutting forces and cutter contact area in MACHpro

A.3 Sensitivity Analysis

The length of the rotor is further shortened to 7.62 mm to meet the satisfied computation time for the repetitive profile simulations in the sensitivity analysis shown as Fig. A.4. The profile deviations caused by the manufacturing misalignment are obtained by adding the geometry errors into the CL files. The misalignment in center distance and setup angle is considered by directly changing their values in the CL file. The pivot angle misalignment is considered by rotating the nominal tool profile $P_t(u_t, v_t)$ by the deviation angle around the Z_t axis. The X_t position error is considered by shifting the TCP along the tool u_t coordinate by the same deviated value.

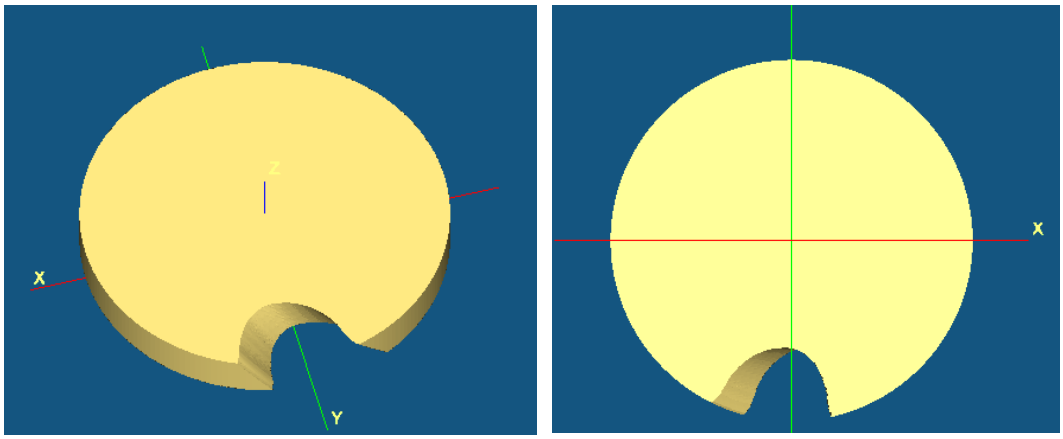

(a) (b)

Figure A.4: Rotor model used in sensitivity analysis

Appendix B

Bibliography

[1] Sham Rane. *Grid generation and CFD analysis of variable geometry screw machines*. PhD thesis, City University London, 2015.

[2] Volker Böß, Berend Denkena, Marc-André Dittrich, Talash Malek, and Sven Friebe. Dexel-based simulation of directed energy deposition additive manufacturing. *Journal of Manufacturing and Materials Processing*, 5(1), 2021.

[3] N. Fang, I.S. Jawahir, and P.L.B. Oxley. A universal slip-line model with non-unique solutions for machining with curled chip formation and a restricted contact tool. *International Journal of Mechanical Sciences*, 43(2):557–580, 2001.

[4] M. Eugene Merchant. Mechanics of the metal cutting process. i. orthogonal cutting and a type 2 chip. *Journal of applied physics*, 16(5):267–275, 1945.

[5] K Ahmadi and A Savilov. Modeling the mechanics and dynamics of arbitrary edge drills. *International Journal of Machine Tools and Manufacture*, 89:208–220, 2015.

[6] Y. Altintas, P. Kersting, D. Biermann, E. Budak, B. Denkena, and I. Lazoglu. Virtual process systems for part machining operations. *CIRP Annals*, 63(2):585–605, 2014.

[7] Kaan Erkorkmaz, Andrew Katz, Yasin Hosseinkhani, Denys Plakhotnik, Marc Stautner, and Fathy Ismail. Chip geometry and cutting forces in gear shaping. *CIRP Annals*, 65(1):133–136, 2016.

[8] F Klocke, C Gorgels, R Schalaster, and A Stuckenberg. An innovative way of designing gear hobbing processes. In *International Conference on Gears*, pages 393–404, 2010.

[9] Nikolaos Tapoglou. Calculation of non-deformed chip and gear geometry in power skiving using a cad-based simulation. *The International Journal of Advanced Manufacturing Technology*, 100(5):1779–1785, 2019.

[10] Jung-Fa Hsieh. Mathematical model and sensitivity analysis for helical groove machining. *International Journal of Machine Tools and Manufacture*, 46(10):1087–1096, 2006.

[11] Changsheng Guo and Yan Tang. Influence of process parameters on screw rotor profiles. *Machining science and technology*, 7(1):105–118, 2003.

[12] Nikola Stosic and Kemal Hanjalic. Development and optimization of screw machines with a simulation model .1. profile generation. *Journal of Fluids Engineering*, 119:659–663, 09 1997.

[13] PJ Arrazola, T Özel, D Umbrello, M Davies, and IS Jawahir. Recent advances in modelling of metal machining processes. *Cirp Annals*, 62(2):695–718, 2013.

[14] M. Eugene Merchant. Basic Mechanics of the Metal-Cutting Process. *Journal of Applied Mechanics*, 11(3):A168–A175, 03 2021.

[15] Xiaoliang Jin and Yusuf Altintas. Slip-line field model of micro-cutting process with round tool edge effect. *Journal of Materials Processing Technology*, 211(3):339–355, 2011.

[16] EH Lee and BW Shaffer. The theory of plasticity applied to a problem of machining. 1951.

[17] M Kaymakci, ZM Kilic, and Y Altintas. Unified cutting force model for turning, boring, drilling and milling operations. *International Journal of Machine Tools and Manufacture*, 54:34–45, 2012.

[18] Serafettin Engin and Yusuf Altintas. Mechanics and dynamics of general milling cutters.: Part i: helical end mills. *International journal of machine tools and manufacture*, 41(15):2195–2212, 2001.

[19] S Engin and Y Altintas. Mechanics and dynamics of general milling cutters.: Part ii: inserted cutters. *International Journal of Machine Tools and Manufacture*, 41(15):2213–2231, 2001.

[20] Derek Yip-Hoi and Xuemei Huang. Cutter/workpiece engagement feature extraction from solid models for end milling. 2006.

[21] K. Weinert, A. Enselmann, and J. Friedhoff. Milling simulation for process optimization in the field of die and mould manufacturing. *CIRP Annals*, 46(1):325–328, 1997.

[22] A. A. G. Requicha and J. R. Rossignac. Solid modeling and beyond. *IEEE Computer Graphics and Applications*, 12(5):31–44, 1992.

[23] Andrew Katz, Kaan Erkorkmaz, and Fathy Ismail. Virtual Model of Gear Shaping—Part I: Kinematics, Cutter–Workpiece Engagement, and Cutting Forces. *Journal of Manufacturing Science and Engineering*, 140(7), 04 2018. 071007.

[24] Pierce McCloskey, Andrew Katz, Luke Berglind, Kaan Erkorkmaz, Erdem Ozturk, and Fathy Ismail. Chip geometry and cutting forces in gear power skiving. *CIRP Annals*, 68(1):109–112, 2019.

[25] Milad Azvar, Andrew Katz, Jacob Van Dorp, and Kaan Erkorkmaz. Chip geometry and cutting force prediction in gear hobbing. *CIRP Annals*, 70(1):95–98, 2021.

[26] Aristomenis Antoniadis. Gear skiving—cad simulation approach. *Computer-Aided Design*, 44(7):611–616, 2012.

[27] DS Sheth and S Malkin. Cad/cam for geometry and process analysis of helical groove machining. *CIRP annals*, 39(1):129–132, 1990.

[28] Changsheng C Guo and Yan Y Tang. Screw rotor profile manufacturability. *Machining science and technology*, 7(1):53–64, 2003.

[29] Machpro. `https://www.malinc.com/products/machpro/`.

[30] E Budak, Y Altintas, and EJA Armarego. Prediction of milling force coefficients from orthogonal cutting data. 1996.